Dynamic flexoelectric instabilities in nematic liquid crystals

E. S. Pikina [1,2] A. R. Muratov [2] E. I. Kats [1] and V. V. Lebedev [1,3]

[1]*Landau Institute for Theoretical Physics*, RAS, 142432, Chernogolovka, Moscow region, Russia
[2]*Institute for Oil and Gas Research*, RAS, 119917, Gubkina 3, Moscow, Russia
[3]*NRU Higher School of Economics*, 101000, Myasnitskaya 20, Moscow, Russia

Electrohydrodynamic phenomena in liquid crystals constitute an old but still very active research area. The reason is that these phenomena play the key role in various applications of liquid crystals and due to the general interest of the physical community in out-of-equilibrium systems. Nematic liquid crystals (NLCs) are ideally representative for such investigations. Our article aims to study theoretically the linear NLCs dynamics. We include into consideration orientation elastic energy, hydrodynamic motion, external alternating electric field, electric conductivity, and flexoelectric polarization. We analyze the linear stability of the NLC film, determining dynamics of perturbations with respect to the homogeneous initial state of the NLC. For the purpose we compute eigenvalues of the evolution matrix for a period of the external alternating electric field. These eigenvalues determine the amplification factors for the modes during the period. The instability occurs when the principal eigenvalue of the evolution matrix becomes unity by its absolute value. The condition determines the threshold (critical field) for the instability of the uniform state. It turns out that one might expect various types of the instability, only partially known and investigated in the literature. Particularly, we find that the flexoelectric instability may lead to two-dimensionally space-modulated patterns exhibiting time oscillations. This type of the structures was somehow overlooked in the previous works. We formulate conditions needed for the scenario to be realized. We hope that the results of our work will open the door to a broad range of further studies. Of especial importance would be a comprehensive understanding of the role of various material parameters and nonlinear effects which is a key step for the rational design of NLCs exhibiting the predicted in this publication multidimensional oscillating in time patterns.

I. INTRODUCTION

A wide variety of pattern-forming instabilities in nematic liquid crystals (NLCs) under the influence of electric field has been extensively investigated already about 50 years, see, e.g., Refs. [1–27]. And many more references can be added. Therefore, one could think that fundamental studies of this phenomenon are exhausted. However, recently the topic was resurrected and attracted much attention from researchers. At least partially because the field has been enriched by observations of localized and propagating excitations in NLCs under external alternating electric field [28–30]. Note that similar phenomena (i.e., localized and propagating excitations) have been observed in different kinds of liquid crystals and under different conditions [31–35].

The observations of Refs. [28–30] were made at the conditions, where the flexoelectric effect plays a crucial role. The flexoelectricity in liquid crystals has been introduced long ago by Meyer and then studied in many works [1–27]. However, the results reported in Refs. [28–35] suggest that the flexoelectric mechanism can bring about a variety of unknown scenarios. The observed in these works localized and propagating excitations suggest that the mechanism behind is based on nonlinear physics in out-of-equilibrium dissipative systems. The first mandatory step to rationalize the observed in these works nontrivial dynamic behavior is to solve the linear dynamic equations for the NLCs in the external AC field. This is the aim of our publication. For the problem under consideration even the analysis of solutions of the linearized equations turns out rather tricky. That is why in this paper we have deliberately focused on the most limited questions of linear stability and postpone the nonlinear step for the further works.

In this work we solve numerically the set of the linear electrohydrodynamic equations in an external alternating electric field. Our scheme includes all essential ingredients of the problem, namely, the Frank elasticity, the hydrodynamic motion, the electric conductivity, and the flexoelectric polarization. In addition, we assume the uniform boundary conditions with strong surface anchoring for the director. The hydrodynamic motion is assumed to be incompressible, the mass density ρ is regarded to be constant, and the incompressibility condition $\nabla \cdot \boldsymbol{v} = 0$ is imposed on the velocity field $\boldsymbol{v}$. The incompressibility condition is explained by small values of Mach number in the hydrodynamic motion that we are interested in.

The linear electrohydrodynamic equations for NLCs are known (see, e.g., Refs. [20,27,36–42]). However, in most of the cited publications above, not all essential ingredients were included into consideration: e.g., hydrodynamic motion or finite (although small) electric conductivity. To be sure that nothing is missing in the previous works (where the linear dynamic equations were constructed by the symmetry arguments) we rederived the equations by the linearization

of the obtained recently [43] by our group complete set of nonlinear dynamic equations of NLCs. It turns out that our set of the linear equations coincides (up to notations) with the equations presented in Ref. [37]. Thus we use the system of linear equations of the nematic, in the form derived by linearization of the complete system of nonlinear equations and solve the equations in the main body of the paper. Partially because in our approach it is essential to separate explicitly the contributions from the ideally insulating NLC. Then the finite conductivity effects are included as a perturbation over small conductivity of the NLC.

In view of time periodicity of the external electric field, the equations of nematodynamics have to be solved in terms of Floquet normal form in time t. Thus the solution is characterized by a set of characteristic exponents (decrements or increments) λ_i, see Refs. [44,45]. We are interested in the dynamic behavior of the NLC on timescales much larger than the period T of the external alternating electric field. The behavior of the amplitudes of the modes on the timescales is described by the factors $\exp(\lambda_i t)$. To establish the set of λ_i, we solve the equations for one period and find the amplification factors $\Lambda_i = \exp(\lambda_i T)$ of the eigenmodes of the evolution operator.

The flexoelectric effect makes the state of the nematic with the homogeneous director field unstable in high-enough external electric fields. The critical electric field, corresponding to the instability threshold, is determined by the condition of zero real part of the main characteristic exponent, related to the critical mode. All other characteristic exponents have negative real parts at the threshold. Our aim is to perform the linear stability analysis and to examine the behavior of the nematic near the instability threshold. Unfortunately, the equations cannot be solved analytically. That is why we investigate their solutions numerically and supplement the numerics by analytic expressions which can be obtained for the pulse-like time-dependent electric field.

We study mainly the simplified model, assuming that all three Frank modules are equal in the director elastic energy, and the only flexocoefficient is taken into account. In addition, we assume that the viscous dissipation energy is characterized by a single viscosity coefficient η (see details in the next section). This approach allows us to bury our ignorance about the actual magnitudes of the many material characteristics of nematics in a few phenomenological parameters. However, even the simplified model enables one to draw general conclusions applying to any NLC. We believe that the model reflects correctly the physics of the dynamic flexoelectric instability. Unfortunately, even the simplified model of the linear electrohydrodynamics of NLCs contains a large number (often poorly known experimentally) of material parameters. Therefore, a complete analysis of such a multiparametric dynamic phase diagram is practically impossible even numerically (and, most importantly, is not very meaningful).

That is why we introduced the simplified model where the number of the parameters is reduced. We believe that the model correctly describes qualitative features of the phenomenon. We aim to draw general qualitative conclusions concerning the character of the dynamic flexoelectric instability. To confirm that our qualitative conclusions are robust with respect to the model assumptions, we discuss also some results obtained by going beyond the simplified model.

We encounter competing bifurcations of the initially uniform director field, leading to the following patterns: (i) stationary stripe structures, (ii) stationary two-dimensionally-modulated structures or oblique rolls, and (iii) oscillating in time two-dimensional structures. Which one of these bifurcations appears upon increasing the external electric field depends on the material parameters and the field frequency ω. The stripe flexoelectric domains, case (i), are well known [10–13]. The oblique rolls from case (ii), were predicted and observed experimentally, see Refs. [20,36–39]. However, scanning the literature, we did not find theoretical predictions or experimental observations of the oscillating patterns in NLCs.

Let emphasize, that it is impossible to determine whether oblique rolls or two-dimensional periodic structures occur above the threshold within the linear stability analysis. Nonlinear terms should be included into consideration to discriminate the possible structures, it is beyond our work. If amplification factors Λ near the instability threshold are real, both structures are possible. It can be shown based on a simple phenomenological description in terms of the critical modes with nonzero components of the wave vector q_x, q_y. Depending on the ratio of two nonlinear contributions in the dynamic equations, either a one-dimensional or two-dimensional pattern is formed.

We solve the complete set of the linear equations for NLCs in the external AC electric field for two cases of the boundary conditions: periodic boundary conditions and more realistic boundary conditions corresponding to the strong planar anchoring energy. As opposed to the static case, where the flexoelectric instability is not observed for homeotropic LC alignment [19], we find that, in the AC electric field, the dynamic flexoelectric instability is possible for both types of boundary conditions examined. For the homeotropic anchoring in (−−) materials, the flexoelectric instability in an AC electric field appears as a secondary instability, following the bend Freedericksz transition (see, e.g., the review paper by Eber *et al.* [46]). For the static (DC electric field) flexoelectric instability, the strength and the type (planar or homeotropic) boundary conditions are very important [19]. However, it is not the case if the frequency of the AC electric field is high, we are interested in our work.

As a result we find the characteristic exponents λ_i determining the amplification factors $\exp(\lambda_i T)$ of the eigenmodes of the equations. At the first step we solve the system under assumption of the periodic boundary conditions. The partial differential equations are reduced to ordinary differential equations (ODEs) in this case. At the second step we use realistic boundary conditions on the nematic film surfaces. We demonstrated that the results obtained in the periodic approach and for the realistic boundary conditions are close if the inequality $(q_{cy}^2 + q_{cx}^2)^{1/2} \gg 1/d$ is satisfied, where (q_{cx}, q_{cy}) are lateral components of the critical wave vector.

To check the generality of our conclusions, we solved the dynamic equations for two types of time-dependent external field: for the harmonic and for the pulsing external electric field (that is the field which is constant during the half of a period and changes its sign at the second half of the period). We have found that all qualitative features of the solutions are the same for the cases.

Unfortunately, we did not find in the literature any experimental results manifesting our main new prediction in this work (oscillating in time two dimensional textures). For example, the results presented in Ref. [37] were obtained for relatively large values of conductivities and low electric-field frequencies, in contrast with our consideration (low conductivity, high frequency). We present the phase diagrams, revealing the parameters needed for realization of our scenario. We hope that the direction of search suggested by our analysis enables one to find a suitable material where the type of instability will be observed.

Our paper is divided into five sections of which this introduction is the first. In Sec. II we introduce the main relations underlying our analysis and the computational scheme. In Sec. III, the linear stability of the system with the periodic boundary conditions in an external alternating electric field is analyzed. We compare the results for the harmonic and for the pulse dependence of the field on time. Section V is devoted to linear stability analysis for a nematic film of finite thickness. The nematodynamic equations are solved with suitable boundary conditions. Our results are outlined in the conclusion. Particularly, we discuss a possibility of the appearance of oscillating-in-time states above the instability threshold. All technical details needed to analyze the dynamics of flexoelectric instability for finite-size systems are presented in Appendix A. We relegated into Appendix B the tables of the results of our computations to compare quantitatively the results obtained for the periodic boundary conditions (with $q_z = \pi/d$) with those for the realistic boundary conditions.

II. GENERAL RELATIONS

Nematic liquid crystals are anisotropic fluids, the anisotropy is described in terms of the director field $\boldsymbol{n}$, that is, the unit headless vector. Distortions of the director fields are associated with the nematic elastic energy

$$\int dV \left\{ \frac{K_1}{2}(\nabla \boldsymbol{n})^2 + \frac{K_2}{2}[\boldsymbol{n}(\nabla \times \boldsymbol{n})]^2 + \frac{K_3}{2}[\boldsymbol{n} \times (\nabla \times \boldsymbol{n})]^2 \right\},$$
(1)

which is called the Frank energy. Here K_1, K_2, K_3 are the Frank modules, typically of the same order.

The electric energy of the nematics is anisotropic as well. Following the general ideology [18,47], it can be written as

$$-\frac{\epsilon_0}{2}\int dV\{\epsilon_\parallel(\boldsymbol{n}\boldsymbol{E})^2 + \epsilon_\perp[E^2 - (\boldsymbol{n}\boldsymbol{E})^2]\},$$
(2)

where $\boldsymbol{E}$ is the electric field, ϵ_0 is the vacuum permittivity, and $\epsilon_\parallel$ and $\epsilon_\perp$ are components of the dielectric permittivity, longitudinal and perpendicular to the director $\boldsymbol{n}$. The degree of the anisotropy is characterized by the difference $\Delta\epsilon = \epsilon_\parallel - \epsilon_\perp$.

In addition, the nematics possess the flexoelectric polarization $\boldsymbol{P}_{fl}$ related to distortions of the director field

$$\boldsymbol{P}_{fl} = e_1\boldsymbol{n}(\nabla \boldsymbol{n}) + e_3(\boldsymbol{n}\nabla)\boldsymbol{n}.$$
(3)

Here e_1, e_3 are flexocoefficients related to splay-like and bend-like deformations of the director field $\boldsymbol{n}$ [8,9,18]. The

flexoelectric energy is of the nematic written as

$$-\int dV \boldsymbol{P}_{fl}\boldsymbol{E}.$$
(4)

Note that, for the homogeneous-in-space electric field $\boldsymbol{E}$, the flexoelectric contribution (4) into the bulk energy of the nematic (i.e., with surface terms neglected) is determined by the single combination $\zeta = e_1 - e_3$.

Dynamics of the nematics is determined by a set of kinetic coefficients. First of all, we should note the director rotational viscosity γ determining kinetics of the director. The quantity has the dimension of the hydrodynamic viscosity coefficients and is usually of the same order. Due to the anisotropy there are five independent viscosity coefficients in the nematic, entering the forth-order viscosity tensor η_{ijkl} [18]. The viscosity coefficients are usually of the same order.

We examine the nematics in the external alternating electric field E. First, we consider the harmonically varying in time electric field $E = E_0 \cos(\omega t)$, where E_0 is the amplitude of the electric field and ω is its frequency. The field is periodic with the period $T = 2\pi/\omega$. Second, we consider the pulsing periodic field consisting of both positive and negative pulses. During a period of duration T its time dependence is

$$E(t) = E_0, \quad 0 < t < T/2, \quad E(t) = -E_0, \quad T/2 < t < T,$$
(5)

where E_0 is the amplitude of the field. The temporal dependence (5) of the external electric field was first considered (within the model neglecting hydrodynamic motion and conductivity) in Ref. [10].

Nematics are weak electrolytes where both positive and negative ions carry the electric current. The density of the electric current $\boldsymbol{j}$ is determined by the directed motion of the ions. Due to the anisotropy of nematics the relation between the electric field $\boldsymbol{E}$ and the density of the electric current is

$$\boldsymbol{j} = \sigma_\parallel\boldsymbol{n}(\boldsymbol{n}\boldsymbol{E}) + \sigma_\perp[\boldsymbol{E} - \boldsymbol{n}(\boldsymbol{n}\boldsymbol{E})],$$
(6)

where $\sigma_\parallel$ and $\sigma_\perp$ are the components of the conductivity longitudinal and perpendicular to the director $\boldsymbol{n}$. The conductivity can be estimated as

$$\sigma \sim \frac{ce^2}{k_B T}D,$$

where D is the diffusion coefficient of the ions, c is their density, e is the electron charge, k_B is Boltzmann constant and T is temperature.

Using the expression for the density of the electric current (6), we ignore contributions to $\boldsymbol{j}$ related to possible inhomogeneities of the space distribution of the ions. Therefore the frequency ω should be much larger than the ions relaxation rate D/r_D^2 where Debye length r_D is estimated as

$$r_D \sim \left(\frac{k_B T \epsilon_0 \epsilon_\perp}{ce^2}\right)^{1/2}.$$

Therefore the condition $\omega \gg D/r_D^2$ can be rewritten as

$$\omega \gg \frac{\sigma}{\epsilon_0 \epsilon_\perp}.$$
(7)

The inequality (7) is assumed to be satisfied in what follows.

We are interested in the flexoelectric instability. To restrict to only this case, it is convenient to avoid other types of electrohydrodynamic instability. In this respect one should distinguish materials with positive and negative signs of the dielectric permittivity difference $\Delta\epsilon = \epsilon_\parallel - \epsilon_\perp$ and of the conductivity difference $\Delta\sigma = \sigma_\parallel - \sigma_\perp$. Correspondingly, there are four classes of the NLCs. These classes are designated as $(--)$, $(-+)$, $(+-)$, and $(++)$, where the first sign in the brackets stands for the dielectric permittivity and the second one stands for the conductivity, see [18].

At increasing the external electric field the $(++)$ and $(+-)$ materials experience the well-known Frederiksz instability, not related to flexoelectricity. The theoretical analysis of electrohydrodynamic instabilities in nematic films and the experimental data [5–8,14–20,25–27,36–39] shows that for the $(-+)$ nematics the instability usually leads to static stripes. At some conditions the instability leads to a two-dimensional pattern of the director field [37]. However, the pattern appears to be stationary as well. It is why in this paper we consider solely the $(--)$ materials.

There is a hierarchy of the relaxation times in NLCs. The slowest mode is related to the director relaxation. Its decrement is determined by the director rotational viscosity γ and the Frank modules K_1, K_2, K_3. The decrement is estimated as Kq^2/γ, where K stands for K_1, K_2, K_3 and q is the characteristic wave vector of the considered mode.

The relaxation rate of the hydrodynamic motion of the nematic at a given wave vector q can be estimated as $\eta q^2/\rho$, where ρ is the mass density, and η estimates the dynamic viscosity coefficients of the nematic. This relaxation rate is much larger, than the director distortion relaxation rate. The ratio of these rates is the dimensionless parameter $K\rho\gamma^{-1}\eta^{-1}$, independent of q. Usually $\gamma \sim \eta$, therefore the parameter can be written as $K\rho\eta^{-2}$. Typically in NLCs it is a small parameter in the range 10^{-4}–10^{-3}[27,36–40,48]. The smallness of the parameter $K\rho\eta^{-2}$ means that, at studying the dynamics of the director distortions, the velocity $\boldsymbol{v}$ of the nematic can be treated in the adiabatic approximation. In other words, the velocity adjusts simultaneously to the director field. The approximation leads to the estimate $v \sim (Kq/\eta)\delta n$ for the velocity, where δn is the director field distortion.

Near the threshold the terms in the equations with the external electric field and with the Frank modules are of the same order. Comparing the Frank energy (1) and the anisotropy of the electric energy (2) we obtain the following relation:

$$|\Delta\epsilon|\epsilon_0 E_c^2 \sim Kq_c^2, \tag{8}$$

which gives the estimate for the wave vector q_c of the critical mode. Here E_c is the amplitude of the external electric field corresponding to the onset of the flexoelectric instability. Comparing then the director relaxation rate $\sim Kq^2/\gamma$ and the field frequency ω, we arrive at the estimate

$$q_c \sim (\gamma\omega/K)^{1/2} \tag{9}$$

for the critical wave vector. Combining the estimates (8) and (9), we find

$$|\Delta\epsilon|\epsilon_0 E_c^2 \sim \gamma\omega. \tag{10}$$

The flexoelectric energy (4) competes with the Frank energy (1). Comparing the energies for the critical values (10)

and (9), we find that their ratio is determined by the factor $\zeta(|\Delta\epsilon|K)^{1/2}$. Thus no flexoelectric instability occurs if ζ is too small. The instability, observed at increasing the external alternating electric field, occurs if the inequality is correct

$$\zeta^2/(|\Delta\epsilon|\epsilon_0 K_1) > C, \tag{11}$$

where C is a constant of order unity. Its value is not universal being dependent on the material parameters of the nematic. The condition (11) is a generalization of the analogous condition for the onset of the flexoelectric instability in the static electric field (the same holds for the pulse field within the model neglecting hydrodynamic motion and conductivity, see Refs. [10–13]). In turn, the conditions (8)–(10) are generalizations of the analogous conditions for the onset of the flexoelectric instability for the pulse field within the model neglecting hydrodynamic motion and conductivity, see Ref. [10].

For the nematic film of finite thickness d, the estimates, formulated above, are correct provided $q_c d \gtrsim 1$. Furthermore, the condition is assumed to be satisfied. Moreover, we consider relatively thick films where $q_c d$ is large. The main qualitative findings of our work are valid for such "thick" films, and all quantitative results for the film of finite thickness are close to those for the sample under periodic boundary conditions.

In our numerical computations we use mainly the simplified model with a single Frank module $K_1 = K_2 = K_3 = K$ and with a single viscosity coefficient η. Namely, we assume that $\eta_1 = \eta_2 = \eta_3 = \eta_4 \equiv \eta$, and $\eta_5 = 0$, see Ref. [43]. It is easy to check that such a choice does not violate the conditions for the positive entropy production, see the conditions in Ref. [18]. We assume $e_3 = 0$ as well. To check generality of the results obtained in the framework of the simplified model we performed also the computations giving up some restrictions of the simplified model, namely, for different Frank modules and for nonzero e_3.

In the framework of the simplified model we deal with the following dimensionless parameters:

$$\eta/\gamma, \quad \Delta\epsilon/\epsilon_\perp, \quad K_1|\Delta\epsilon|\epsilon_0/\zeta^2, \tag{12}$$

controlling the character of the instability. All the subsequent general conclusions can be formulated in terms of the dimensionless parameters.

Note that not all relevant for the NLC dynamic parameters are reliably known experimentally even for the so-to-speak standard [e.g., 4-methoxybenzylidene-4′-butylaniline (MBBA)] nematics. All the more it is true for some recently synthesized materials, see, e.g., Refs. [28–35]. Thus one may play with the material parameters (of course within the limits of physically acceptable values). Following this way, we predict the region of parameters where the scenario of the dynamic flexoelectric instability is realized, related to oscillating-in-time patterns.

Linear dynamic equations of nematic liquid crystals

To be specific, in what follows we consider the nematic film enclosed by two parallel plates and chose the X and Y axes of the reference system along the plates. We assume that the external alternating electric field is directed along the Z

axis, and that without the external electric-field director **n** is aligned everywhere along the X axis. Experimentally, the geometry can be achieved by special preparing the surfaces of the plates guaranteeing that **n** is directed along X axis there. Above the instability threshold the director field **n** loses its homogeneity.

Since the nematic film is assumed to be homogeneous in the X-Y plane, one can examine modes with the harmonic dependence $\exp(iq_x x + iq_y y)$ of all varying quantities. The flexoelectric instability occurs at a finite wave vector $\boldsymbol{q} = (q_x, q_y)$. The stripe structure of the director field above the stability threshold corresponds to $q_x = 0$ or to $q_y = 0$ for the critical mode. If both components of the wave vector of the critical mode are nonzero, then two-dimensional modulated structures can be realized.

We perform the linear stability analysis of the nematic liquid crystal dynamics in the presence of an alternating electric field. The linear electrohydrodynamic equations for NLCs are known (see, e.g., Refs. [20,27,36–42]). The equations can also be derived by the linearization of the complete set of nonlinear dynamic equations of NLCs obtained recently [43] by our group. It turns out that our set of the linear equations coincides (up to notations) with the equations presented in Ref. [37]. Thus we use the system of linear equations of the nematic in the form derived by linearization of the complete system of nonlinear equations [43].

Within our simplified model ($K_1 = K_2 = K_3 = K$, $e_3 = 0$ and a single viscous coefficient η), one finds the following system of equations for the fields with the dependence $\propto \exp(iq_x x + iq_y y)$:

$$\partial_t n_y = iq_x v_y + \frac{1}{\gamma}\left[K(\partial_z^2 - q^2)n_y - i\zeta q_y n_z E(t) - \zeta q_x q_y \Phi\right], \tag{13}$$

$$\partial_t n_z = iq_x v_z + \frac{1}{\gamma}\Big[K(\partial_z^2 - q^2)n_z + i\zeta q_y n_y E(t) \\ + \Delta\epsilon\epsilon_0 E(t)^2 n_z - i\Delta\epsilon\epsilon_0 E(t)q_x\Phi + i\zeta q_x\partial_z\Phi\Big], \tag{14}$$

$$\rho\partial_t v_y = \eta(\partial_z^2 - q^2)v_y - iq_y\Pi - iK(\partial_z^2 - q^2)q_x n_y, \tag{15}$$

$$\rho\partial_t v_z = \eta(\partial_z^2 - q^2)v_z - \partial_z\Pi - iK(\partial_z^2 - q^2)q_x n_z \\ - \epsilon_\perp\epsilon_0 E(t)(\partial_z^2 - q^2)\Phi, \tag{16}$$

$$\partial_t\Big[\epsilon_\parallel\epsilon_0 q_x^2\Phi + \epsilon_\perp\epsilon_0(q_y^2 - \partial_z^2)\Phi \\ - iq_x(\Delta\epsilon\epsilon_0 n_z E(t) + i\zeta q_y n_y + \zeta\partial_z n_z)\Big] \\ = -\sigma_\parallel q_x^2\Phi - \sigma_\perp(q_y^2 - \partial_z^2)\Phi - i\Delta\sigma E(t)q_x n_z. \tag{17}$$

Here $q^2 = q_x^2 + q_y^2$; n_y, n_z are the components of the director **n**, describing its deviations from the equilibrium orientation; and v_y, v_z are the components of the velocity. We introduce also $\delta\boldsymbol{E} = -\nabla\Phi$ as a perturbation of the homogeneous electric field. The parameter Π, figuring in the equations (15) and (16), is the effective pressure, satisfying the relation

$$(\partial_z^2 - q^2)\Pi = i\zeta E(t)q_x^3 n_z + \zeta q_x^4\Phi + K(\partial_z^2 - q^2) \\ \times q_x(q_y n_y - i\partial_z n_z) - \epsilon_\perp\epsilon_0 E(t)\partial_z(\partial_z^2 - q^2)\Phi. \tag{18}$$

The condition (18) is a consequence of the incompressibility condition $iq_x v_x + iq_y v_y + \partial_z v_z = 0$. The same condition enables one to exclude v_x from the set of the dynamic variables.

Modification of the equations in the case of three different Frank moduli is discussed in Appendix A.

One has to solve the set of the linear equations (13)–(18) supplemented by suitable boundary conditions. The natural boundary conditions for the fields n_y, n_z, v_y, v_z, Φ are zero Dirichlet boundary conditions. Physically, they are related to fixing director at the surface by the strong anchoring energy to nonslipping boundary conditions for the velocity and to fixing the electric potential at the boundaries of the plates. The last condition is provided by the conducting electrodes on the surfaces of the nematic film. The zero Dirichlet conditions have to be supplemented by an additional boundary condition $\partial_z v_z = 0$, following from the incompressibility condition $iq_x v_x + iq_y v_y + \partial_z v_z = 0$ and zero values of the components v_x, v_y at the boundaries. Thus we arrive at the boundary conditions for the film of thickness d, imposed at $z = \pm d/2$:

$$n_y(z = \pm d/2) = 0,$$
$$n_z(z = \pm d/2) = 0,$$
$$\Phi(z = \pm d/2) = 0,$$
$$v_y(z = \pm d/2) = 0,$$
$$v_z(z = \pm d/2) = 0,$$
$$\partial_z v_z(z = \pm d/2) = 0. \tag{19}$$

From the formal point of view, the additional condition $\partial_z v_z(z = \pm d/2) = 0$ is needed to specify the generalized pressure Π, see Eq. (18).

The system of equations (13)–(17) describes a set of modes, possessing a complicated temporal behavior in the external alternating electric field. One can extract eigenmodes, that are characterized by returning to their spatial structure after a period T of the external field up to a factor Λ_i, which can be called the amplification factor of the eigenmode. We introduce also the characteristic exponents λ_i related to the amplification factors Λ_i through $\Lambda_i = \exp(\lambda_i T)$. The exponents λ_i determine the behavior of the eigenmodes on temporal scales much larger than T via the factors $\exp(\lambda_i t)$. The equations (13)–(18) written in terms of the variables n_y, in_z, iv_y, v_z, Φ, and Π have real coefficients. That is why the characteristic exponents λ_i must be all real or contain some complex conjugated pairs.

One easily checks that the set of the linear electrohydrodynamic equations (13)–(18) is invariant under the following transformations:

$$q_y \to -q_y, \quad n_z \to -n_z, \quad n_y \to n_y,$$
$$v_z \to -v_z, \quad v_y \to v_y, \tag{20}$$

and

$$q_x \to -q_x, \quad n_z \to n_z, \quad n_y \to n_y,$$
$$v_z \to -v_z, \quad v_y \to -v_y, \quad \Pi \to -\Pi. \tag{21}$$

Note that even beyond the assumptions of our simplified model the complete set of the linear nematodynamic equations remains invariant under the transformations (20)

and (21). The symmetry of the equations under the transformations (20) and (21) lead to the conclusion that the characteristic exponents $\lambda_i(q_x, q_y)$, do not change upon changing sign of q_x or q_y.

The modes described by the system of equations (13)–(17), all decay below the instability threshold. Above the threshold, a mode (or modes) that can be called the critical one becomes unstable. Evidently, the actual patterns of the nematic above the threshold cannot be analyzed in the framework of the linear approximation (above the threshold the amplitude of the mode grows and the linear approximation is violated). Nevertheless, some general conclusions concerning the state can be derived from the analysis of the system at the threshold.

One can get some insight on various structures above the threshold phenomenologically. For the real amplification factor at fixed q_z in the vicinity of the threshold the instability occurs for the modes with nonzero components of the wave vectors q_x, q_y. Introducing two complex amplitudes describing the modes one finds that the solution with one nonzero amplitude corresponds to oblique rolls whereas the solution with two nonzero amplitudes corresponds to a two-dimensional periodic structure [49].

Near the instability threshold the only third-order terms in the dynamical equations should be taken into account, if the terms stabilize the solution of the equations. In the case the amplitude of the inhomogeneous contribution to the director field is small near the threshold. Then finally the only spatial harmonic survives with the wave vector $\boldsymbol{q}$, corresponding to the maximum value of Re$\lambda_c(\boldsymbol{q})$, where λ_c is the characteristic exponent of the critical mode. Near the threshold $|\lambda_c| \ll \omega$ and, consequently, the slow dynamics of the director patterns is determined just by the critical characteristic exponent λ_c. If Im$\lambda = 0$, then the pattern is stationary. Of course, the stationary behavior occurs on the timescale much larger than the period T of the external alternating electric field, whereas oscillations of the pattern with the period T are omnipresent.

Thus there are different possibilities related to the value of the characteristic exponent $\lambda(q_x, q_y)$ of the critical mode. If Im$\lambda = 0$ then the stationary patterns of the director field $\boldsymbol{n}$ are realized above the threshold, whereas the case Im$\lambda \neq 0$ leads to the possibility of dynamic (oscillating in time) two-dimensional structures above the instability threshold. To avoid a misunderstanding, we stress again that, speaking about the stationary or oscillating regimes, we imply timescales much larger than the period T of the external alternating electric field.

If Im$\lambda \neq 0$, then the critical mode oscillates with time. Thus we arrive at the traveling wave described by the factor $\exp(i\text{Im}\lambda t + i\boldsymbol{qr})$. One might encounter two or four plain waves, depending on the arrangement of the values of critical wave vectors in $\boldsymbol{q}$ space. Then the nematic pattern appearing as a result of the instability consists of some traveling or standing waves, depending on conditions at the plates limiting the NLC sample. We are especially interested in the possibility and aim to establish conditions for its realization. Our detailed analysis based on the results of numerical computations is presented in subsequent sections.

Some words about the mechanism of appearing the oscillating critical mode are in order. We assume that the conductivity of the nematic is relatively small; that is, it satis-

fies the inequality (7). Then, as it follows from Eqs. (13)–(17), there is a slowly decaying "potential" mode with Re$\lambda T \ll 1$. Indeed, in the limit $\sigma_\perp, \sigma_\parallel \to 0$ the quantity in the square brackets on the left-hand side of Eq. (17) is unchanged during the electric-field period, which corresponds to the condition $\lambda = 0$ for the mode. For finite $\sigma_\perp, \sigma_\parallel$ we obtain $|\lambda| \sim \sigma/(\epsilon_0 \epsilon_\perp)$, explaining the inequality Re$\lambda T \ll 1$ for the "potential" mode, following from Eq. (7).

The flexoelectric instability implies that the director dynamics is also a "soft" mode. Upon approaching the threshold the value Reλ for the mode tends to zero. Therefore, near the threshold there occurs a hybridization of the "director" and of the "potential" modes. The hybridization can lead to forming two mixed modes with complex conjugated characteristic exponents λ, then Im$\lambda \neq 0$. At some conditions the mixed modes survive up to the instability threshold. Then λ has a nonzero imaginary part at the threshold. We examine the conditions needed for realization of this scenario.

Let us stress that in our model the director modes and hydrodynamic modes are coupled via the kinetic lambda term, see Eqs. (13)–(17). This coupling is a crucial ingredient of our scenario of the flexoelectric instability.

We intend to give a general view on the dynamic flexoelectric instability. Obviously, it is impossible to scan the multidimensional space of the material parameters characterizing the nematic. That is why we simplify the description, reducing the number of the parameters. Of course, to simulate the properties of a specific nematic, one should restore the complete equations with all phenomenological material coefficients taken into account. We do believe that our approach gives the qualitatively correct general picture (e.g., types of the instability and their arrangement on the "phase diagram" plotted in terms of the key parameters). To justify our belief we have performed computations with three different Frank moduli, and two flexoelectric coefficients. We found that, in this case, the qualitative features of the phenomenon (the topology of the "phase diagram" and the scaling laws) remain the same as in our simplified model.

III. FLEXOELECTRIC INSTABILITY IN CASE OF PERIODIC BOUNDARY CONDITIONS

Here we consider the periodic in z setup, enabling us to reduce the partial differential equations to the ordinary differential equations and to avoid difficulties related to the account of the boundary conditions (19). As we already noted, the approach allows one to scan quickly a wide range of material parameters to find the most interesting regions. If it is necessary, later the parameters can be examined in more detail for the nematic sample with the realistic boundary conditions (19). The corresponding analysis is presented in Sec. V.

Note that the case of homeotropic LC alignment in the cell of the ($--$) material under AC electric field differs from the situation with the boundary conditions (19). In the homeotropic case the flexoelectric instability appears as a secondary instability, following the bend Freedericksz transition (see, e.g., the review paper by Eber *et al.* [46]). The electric field E_F at which the Freedericksz transition occurs can be

estimated from the standard relation

$$\epsilon_0 |\Delta\epsilon| E_F^2 \sim K/d^2.$$

In the case considered in our paper, the critical electric field E_c at which the flexoelectric instability takes place is determined by the formulas (8)–(10). Our computations suggest that the dynamic flexoelectric instability occurs when the lateral critical wave vector of the most unstable mode (q_{cx}, q_{cy}) satisfies the inequality $(q_{cy}^2 + q_{cx}^2)^{1/2} d \gg 1$. Then according to the estimates $E_c \gg E_F$. At the condition the behavior of the substance near the flexoelectric instability in the boundary layers of thickness $\sim q_c^{-1}$ is sensitive to the boundary conditions whereas its behavior in the rest of volume is independent of them. That is why our results are not sensitive to the boundary conditions, including the homeotropic or oblique ones. We confirmed the assertion by comparing the periodic setup with the case of the strong parallel anchoring of the director. Note that, for the static field the flexoelectric instability occurs at $q_c \sim d^{-1}$ and is sensitive to the boundary conditions.

We demonstrate in Sec. V and in Appendix B, that the results for the case of periodic boundary conditions (at $q_z = \pi/d$) and for the case of the realistic boundary conditions (19) are close. The fact is justified by the inequality $(q_{cy}^2 + q_{cx}^2)^{1/2} \gg 1/d$.

For the case of periodic boundary conditions the set of equations (13)–(17) admits a solution, which is a linear combination of $\cos(q_z z)$ and $\sin(q_z z)$, where q_z is an arbitrary parameter. Then the system of equations (13)–(17) are reduced to the ordinary differential equations for the coefficients at $\cos(q_z z)$ and $\sin(q_z z)$. In terms of the variables n_y, in_z, iv_y, v_z, Φ, and Π, the equations have real coefficients. That is why the amplification factors Λ_i or the characteristic exponents λ_i are either real or form pairs of complex conjugated values. We fix q_z and find q_x and q_y corresponding to the critical mode, first achieving at the flexoelectric instability.

Alternatively one can look for a solution of the system (13)–(17) proportional to $\exp(iq_z z)$. Then the equations, following from Eqs. (13)–(17) for the periodic BC case can be simply rewritten, see Appendix A. After substituting the expression (A6) into equations (A1)–(A5) they are reduced to the form

$$\frac{d\boldsymbol{f}}{dt} = \hat{\Gamma}\boldsymbol{f}, \tag{22}$$

where $\boldsymbol{f}$ is the vector with the components n_y, n_z, v_y, v_z, Φ, and $\hat{\Gamma}$ is the matrix 5×5 with components periodically varying as time t goes.

As we noted, in NLCs the hydrodynamic flow degrees of freedom are much faster than the director mode. Therefore the velocity in the slow critical mode can be examined in the adiabatic approximation. That means that the time derivatives in the equations (A3), (A4) for v_y, v_z can be neglected. Then the velocity components can be expressed from the expressions via n_y, n_z, Φ. Substituting the expressions into Eqs. (A1), (A2), (A5) we find the equation of the form (22) for the three variables n_y, n_z, Φ. Then we arrive at the 3×3 matrix $\hat{\Gamma}$. We use both approaches, with the matrix 5×5 and with the matrix 3×3. The results, obtained in the framework of the approaches, appear to be the same.

One technical comment is in order here. The characteristic relaxation times of the essential dynamic modes (director, velocity, and potential modes) are strongly different. Therefore the computation of the evolution matrix 5×5 requires the solution of so-called rigid system of differential equations [50], which could create some problems for numerical computations. This is why we use both approaches, with the matrices 5×5 and the matrices 3×3, to be sure that the numerical results are correct.

We solve numerically the equation (22) on a period to find the evolution matrix $\hat{W}$:

$$\boldsymbol{f}(t + T) = \hat{W}\boldsymbol{f}(t). \tag{23}$$

The evolution matrix $\hat{W}$ is independent of time t thanks to periodicity of the matrix Γ. The eigenvalues of the matrix $\hat{W}$ are no other than the amplification factors Λ_i of the eigenmodes of the problem. Note that for n periods

$$\boldsymbol{f}(t + nT) = (\hat{W})^n \boldsymbol{f}(t). \tag{24}$$

The eigenvalues of the matrix $(\hat{W})^n$ are Λ_i^n. Therefore, to better distinguish the critical mode, it is worth examining the evolution determined by Eq. (22) on a few periods.

To find the evolution matrix $\hat{W}$ one can take as initial values $\boldsymbol{f}$ in Eq. (23) the vectors $(1, 0, 0, \dots)$, $(0, 1, 0, \dots)$, ... Then the corresponding vectors $\boldsymbol{f}(t + T)$ (found numerically) constitute the evolution matrix $\hat{W}$. The procedure can be conducted both for the matrices 5×5 and 3×3, and is directly generalized for the evolution on some periods. After computing the evolution matrix $\hat{W}$ we find its eigenvalues Λ_i and then the characteristic exponents from $\Lambda_i = \exp(\lambda_i T)$.

We are interested in the principal modes, i.e., the modes with maximal real part of the characteristic exponents λ_i, relevant for examining the flexoelectric instability. The oscillating in time regime of the critical mode is realized if there exist two modes characterized by complex conjugated values of the characteristic exponents with nonzero imaginary parts. Note that at $q_x = 0$ the system of the equations (A1) and (A2) for the components n_y, n_z of the director field is decoupled from the other equations. Then the evolution of n_y, n_z is governed by a Hermitian matrix 2×2. Therefore the characteristic exponents λ_i related to the director mode are real in this case. Since just the director mode is responsible for the flexoelectric instability, we conclude that the oscillating regime cannot be realized at $q_x = 0$.

To simplify the dynamic analysis, one often neglects the hydrodynamic flow (see, e.g., Ref. [40]). In the case we stay with the three variables n_y, n_z, Φ. Although the matrix, determining the time derivative of the variables is not Hermitian, we did not find a nonzero imaginary part of λ_1 in this case. Thus our results suggest that an account of the hydrodynamic degrees of freedom is crucial for achieving the regime with the oscillating in time critical mode.

Pulsing external electric field

We analyze mainly the external harmonically varying electric field $E = E_0 \cos(\omega t)$. To check whether the obtained results are robust we investigate also the pulsed form (5) of the alternating external electric field. The case enables one to examine the flexoelectric instability semi-analytically. As

for the harmonically varying field, we study solutions of the system of the dynamic equations (A1)–(A5) during a period of the pulsing field. The evolution matrix $\hat{W}$ is collected from the solutions for the initial vectors $(1, 0, 0, \dots)$, $(0, 1, 0, \dots)$, ... as well.

For the pulsing field (5) the dynamic equations (A1)–(A5) during the time intervals $0 < t < T/2$ and $T/2 < t < T$ are the sets of linear differential equations with constant coefficients. Thus any solution of such system is a sum of the functions $\propto \exp(pt)$, where the set of the five exponents p_α can be obtained analytically. The temporal dependencies of the coefficients n_y, n_z, v_y, v_z, Φ during the first half-period are determined by the five initial conditions $(1, 0, 0, \dots)$, $(0, 1, 0, \dots)$, ... To find the t dependence of the coefficients n_y, n_z, v_y, v_z, and Φ during the second half-period, one has to use the continuity conditions at $t = T/2$ for the variables n_y, n_z, v_y, v_z and of the variable

$$-\epsilon_\parallel q_x^2 \Phi - \epsilon_\perp \left(q_y^2 + q_z^2\right)\Phi + iq_x \Delta\epsilon\, n_z E,$$

as it follows from Eqs. (A1)–(A5).

As a result of the procedure, we find n_y, n_z, v_y, v_z, Φ at $t = T$ for all five initial conditions. Thus the quantities, constituting the evolution matrix $\hat{W}$, can be found analytically. To find the eigenvalues of $\hat{W}$ (amplification factors) Λ_i one has to solve the characteristic equation $\det(\hat{W} - \Lambda) = 0$. The equation is too complicated to be solved analytically. However, the equation can be easily solved numerically. This is the only numerical step needed to investigate the dynamic flexoelectric instability in the pulsating electric field for the case of periodic boundary conditions.

Our computations show that the results for the pulsing field agree well with the corresponding results for the harmonically varying external field. The threshold value of the amplitude of the pulsing field is approximately two times smaller that the amplitude of the harmonic field.

IV. POSSIBLE TYPES OF INSTABILITY

Here we illustrate different types of instability noted in Sec. II by presenting results of the numerical computations for suitable values of the material parameters. In general the periodic in time external AC electric field is considered in this section. We draw the values of the amplification factor Λ of the critical mode near the instability threshold as a function of the lateral wave vector (q_x, q_y) at a given q_z. It is chosen to be less than the lateral wave vector.

Let start with discussing the case of stationary stripes. The case is most easily realized provided the instability occurs at $q_x = 0$, $q_y \neq 0$. As we already noted, in the case the critical mode has real Λ. Therefore in this regime the stripe structure arises above the instability threshold with the stripes oriented along the X axis. The case is realized if the dimensionless parameters (12) are relatively large.

To illustrate the statement we present our numeric results for the parameters

$$\eta/\gamma = 1, \quad \Delta\epsilon/\epsilon_\perp = -0.15, \quad K_1|\Delta\epsilon|\epsilon_0/\zeta^2 = 0.091.$$

The complete set of the parameters used for the computations is presented in the caption for Fig. 1, where the dependencies on q_x, q_y of the amplification factors Λ of two principal
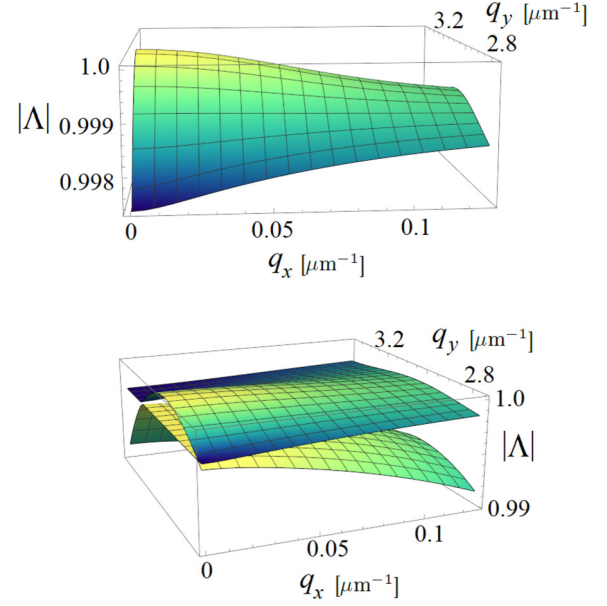
FIG. 1. The dependence of the amplification factors Λ of two principal modes on q_x and q_y for $\omega = 2\pi \times 510$ s^{-1} : $\Lambda = 1.00$ at $E_{bc} = 3.73 \times 10^6$ V/m, $q_z = 0.04$ μm^{-1}, $\sigma_\perp = 1$ s^{-1} $= 10^{-10}$ Ω^{-1}m^{-1}, $\Delta\sigma = -0.2\sigma_\perp$, $K = 7 \times 10^{-12}$ N, $\zeta = 9.2 \times 10^{-4}$ SGSE units $= (9.2/3) \times 10^{-11}$ C m^{-1}, $\epsilon_\perp = 9.2$, $\Delta\epsilon = -4\pi \times 0.11$, $\gamma = 0.06$ Pa s, $\eta = 0.06$ Pa s.

modes are presented near the instability threshold. Besides the simple stripe structure some more complicated stationary structures can be realized above the instability threshold. They are realized if the instability is achieved at $q_x \neq 0$, $q_y \neq 0$. The possibility is discussed, e.g., in Refs. [37–39]. In this case at the instability threshold there are four wave vectors $\pm q_x$, $\pm q_y$ corresponding to $\Lambda = 1$. Above the instability threshold some stationary periodic two-dimensional director pattern can occur. Alternatively, an oblique stripe structure can arise. The choice depends on the character of nonlinearity and is beyond the linear stability analysis.

To illustrate the possibility, we present numeric results for the parameters

$$\eta/\gamma = 0.82, \quad \Delta\epsilon/\epsilon_\perp = -0.214, \quad K_1|\Delta\epsilon|\epsilon_0/\zeta^2 = 0.073,$$

in Fig. 2(a), and

$$\eta/\gamma = 0.53, \quad \Delta\epsilon/\epsilon_\perp = -0.214, \quad K_1|\Delta\epsilon|\epsilon_0/\zeta^2 = 0.049,$$

in Fig. 2(b). The complete set of the parameters used for the computations is presented in the caption to Figs. 2(a) and 2(b).

The next case that can take place at the instability, is related to the oscillating director pattern above the instability threshold. It is realized if two critical modes with the complex conjugated amplification factors Λ appear at the instability threshold, that is achieved at $q_x \neq 0$, $q_y \neq 0$. The case is realized at small enough parameters (12). Such situation probably may occur in nematic materials exhibiting phase transitions into various ferroelectric structures, see Refs. [8,51–54].

As an illustration of this possibility, we present numerical results for the following dimensionless parameters

$$\eta/\gamma = 1, \quad \Delta\epsilon/\epsilon_\perp = -0.052, \quad K_1|\Delta\epsilon|\epsilon_0/\zeta^2 = 0.095$$
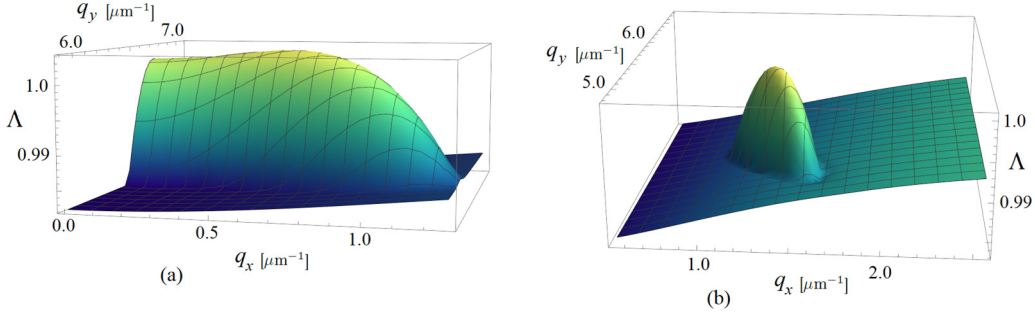
FIG. 2. The dependencies of the amplification factors Λ_1 and Λ_2 of two principal modes on q_x, q_y at $\omega = 2\pi \times 500$ s^{-1}, $q_z = 0.41$ μm^{-1}, $K_1 = 7 \times 10^{-12}$ N, $K_2 = 5 \times 10^{-12}$ N, $K_3 = 5 \times 10^{-12}$ N, $\epsilon_\perp = 14$, $\Delta\epsilon = -3$, $\sigma_\perp = 10$ s$^{-1} = 10^{-9}$ Ω^{-1} m^{-1}, $\Delta\sigma = -0.2\sigma_\perp$, $\gamma = 0.066$ Pa s, (a) $\Lambda = 1.0038$ at $E_{bc} = 1.86 \times 10^6$ V/m for $\zeta = (15.16/3) \times 10^{-11}$ C m^{-1}, $\eta = 0.054$ Pa s; (b) $\Lambda = 1.0006$ at $E_{bc} = 1.46 \times 10^6$ V/m for $\zeta = (18.5/3) \times 10^{-11}$ C m^{-1}, $\eta = 0.035$ Pa s.

in Fig. 3 for $q_z = 0.39$ μm^{-1}, where the real and the imaginary parts of the complex amplification factor Λ of the degenerated modes are presented. The complete set of parameters used for the simulation is presented in the caption to Fig. 3.

We checked that the oscillating regime can be realized for the case of different Frank modules and two different flexoco-efficients. The case is illustrated in Fig. 4. The equations used for the computations can be found in Appendix A, Eqs. (A20) and (A21). As it is seen from Fig. 4, the absolute values of the amplification factor Λ of two principal modes has two competing maxima, one of which is narrow and corresponds to complex Λ, whereas the second one is wide and corresponds to real Λ (though with $q_x \neq 0$). Such possibility can be easily realized for the case of different Frank modules.

A. Phase diagram

One cannot study numerically the complete multidimensional phase space, and anyway it would be not very instructive. To gain a better understanding and some flavor of what can happen, it is beneficial to study the effects of the parameters chosen as selectively as possible. One of the way to explore the found above instabilities within the simplified model is to look for a plane of two parameters, the viscosity coefficient η and the flexoelectric coefficient ζ. The results are presented as "phase diagrams" plotted in terms of the dimensionless parameters η/γ and $K\epsilon_0|\Delta\epsilon|/\zeta^2$. We put a series of the points to the diagrams, where the character of the critical mode is determined numerically. In the diagrams

the star $*$ designates the critical phase with $q_x = 0$ and real Λ, the open circle $\circ$ designates the phase with $q_x \neq 0$ and real Λ, and the bullet $\bullet$ designates the phase with $q_x \neq 0$ and complex Λ.

First, we take $K_1 = K_2 = K_3 = 4 \times 10^{-12}$ N, $\sigma_\perp = 10$ s^{-1}, $\Delta\sigma = -2$ s^{-1}, $q_z = \pi/8$ μm^{-1}, $\epsilon_\perp = 14$, $\Delta\epsilon = -0.8\pi$, $\gamma = 0.06$ Pa s, $\omega = 1000\pi$ s^{-1}. For the sinusoidal external field the results are presented in Fig. 5, where we see all three possibilities. If both dimensionless parameters are large, the critical mode has $q_x = 0$. At this condition the amplification factor Λ is real. At the increase of ζ, i.e., at the decrease of $K|\Delta\epsilon|/\zeta^2$, the wave vector q_x of the critical mode becomes $q_x \neq 0$ and the amplification factor Λ remains real, if η/γ is moderate. Finally at decrease of η we pass to the critical mode with $q_x \neq 0$ and complex amplification factor Λ.

To check the "robustness" of the phase diagram presented in Fig. 5 we conduct an analogous investigation for the pulsing external field, see Eq. (5). The material parameters are the same as above. The results are presented in Fig. 6. The general shape of this diagram is analogous to the diagram for the harmonic field, although the position of transition lines is different. For example, the transition to the phase where the critical mode with $q_x \neq 0$, real Λ takes place at larger values of ζ. The amplitude of the threshold external field for the pulsing field is smaller than for the harmonically varying field.

The results presented above were obtained within our simplified model. The model is formulated with several assumptions (equal Frank constants, one flexoelectric coefficient, and a single viscosity coefficient), driven by pure desire
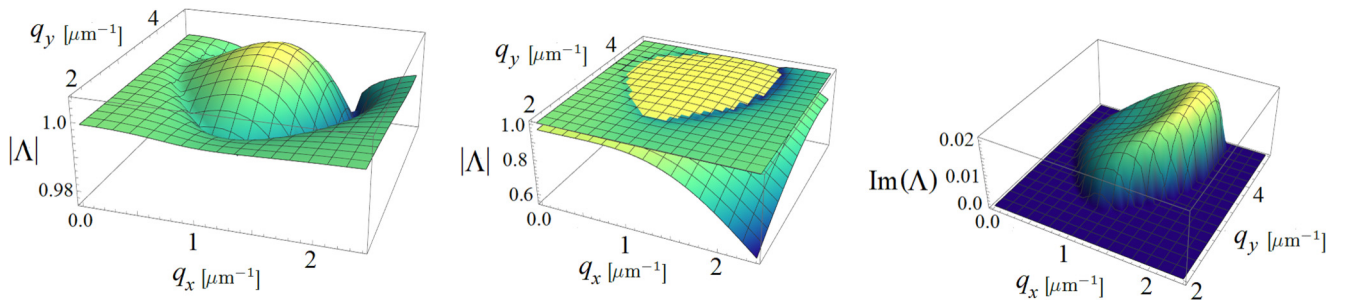
FIG. 3. The dependencies of absolute value of amplification factor Λ of two principal modes and the imaginary part of Λ_1 on q_x and q_y for $\omega = 2\pi \times 500$ s^{-1}: $\Lambda = 1.0065 \pm i0.013$ at $E_{bc} = 3.94 \times 10^6$ V/m for $q_z = 0.39$ μm^{-1}, $\sigma_\perp = 1$ s$^{-1} = 10^{-10}$ Ω^{-1} m^{-1}, $\Delta\sigma = -0.2\sigma_\perp$, $K = 4 \times 10^{-12}$ N, $\zeta = (6.5/3) \times 10^{-11}$ C m^{-1}, $\epsilon_\perp = 24$, $\Delta\epsilon = -4\pi \times 10^{-1}$, $\gamma = 0.06$ Pa s, $\eta = 0.06$ Pa s.
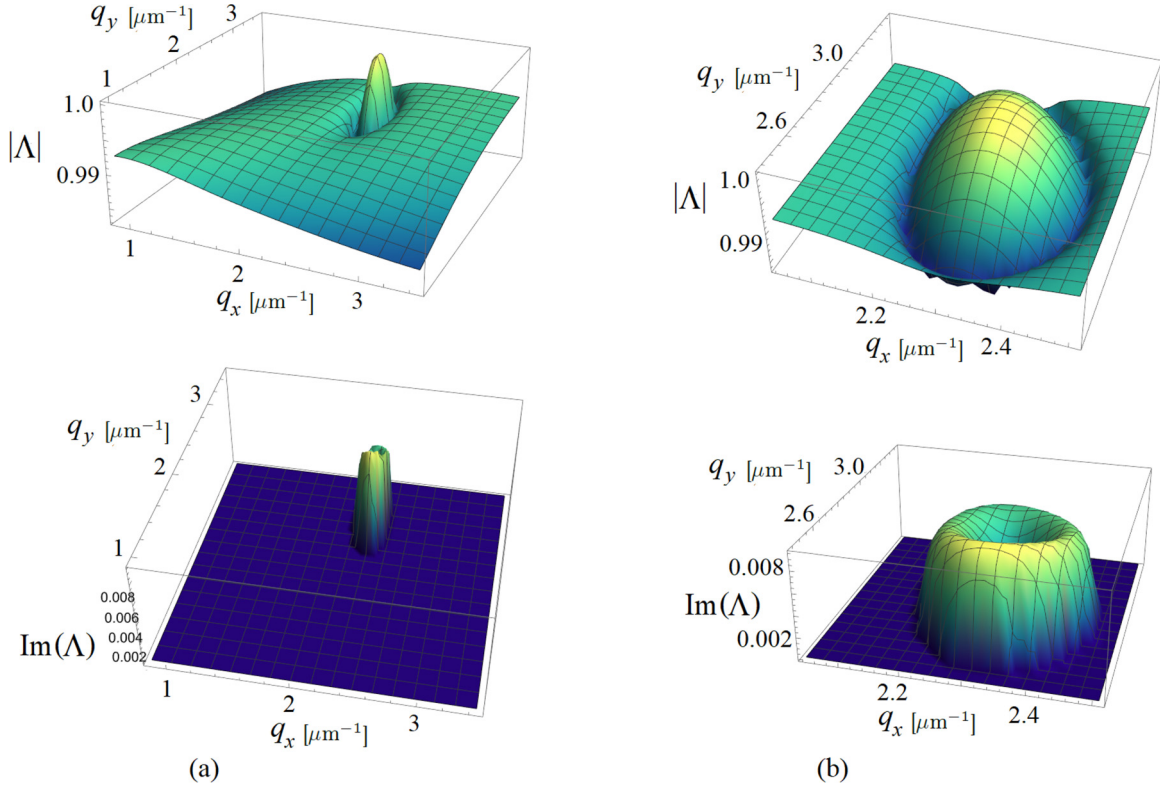
FIG. 4. Dispersion laws near the threshold. The dependence of modules of amplification factor Λ_1 and imaginary part of Λ_1 of main mode on q_x and q_y for $\omega = 2\pi \times 500 \text{ s}^{-1}$. $\Lambda = 1.00141 \pm i0.001$ at $E_{bc} = 0.65 \times 10^6$ V/m for $q_z = 0.4 \ \mu\text{m}^{-1}$, $\sigma_\perp = 0.3 \ \text{s}^{-1} = 0.3 \times 10^{-10} \ \Omega^{-1} \text{m}^{-1}$, $\Delta\sigma = -0.7\sigma_\perp$, $K_1 = 7 \times 10^{-12}$ N, $K_2 = 5 \times 10^{-12}$ N, $K_3 = 5 \times 10^{-12}$ N, $\zeta = (34/3) \times 10^{-11}$ C m^{-1}, $e_3 = (34/3) \times 10^{-11}$ C m^{-1}, $\epsilon_\perp = 14$, $\Delta\epsilon = -3$, $\gamma = 0.066$ Pa s, $\eta = 0.015$ Pa s.

to make formulas simpler. We do believe that more realistic description will not affect our qualitative conclusions, and transparency is worth a few oversimplifications. To illustrate our believe we compute more complex phase diagram for three different Frank modules, $K_1 = 7 \times 10^{-12}$ N, $K_2 = K_3 = 5 \times 10^{-12}$ N. The results are presented in Fig. 7, the complete set of parameters used for the computations is presented in the caption to the figure. We see that the relative position of the three regions remains the same, although the borders between

the phases are different. The phase regions have nontrivial form. And one can see the possibility of the instability, related to the oscillating director pattern. The results demonstrate universality of the phase diagram topology.

It is worth noting also an interesting and useful work [12] illustrating the quantitative relevance (for the static flexo-electric instability) to take into account three Frank moduli and two flexoelectric coefficients. The same (the quantita-tive relevance of three elastic moduli and two flexoelectric
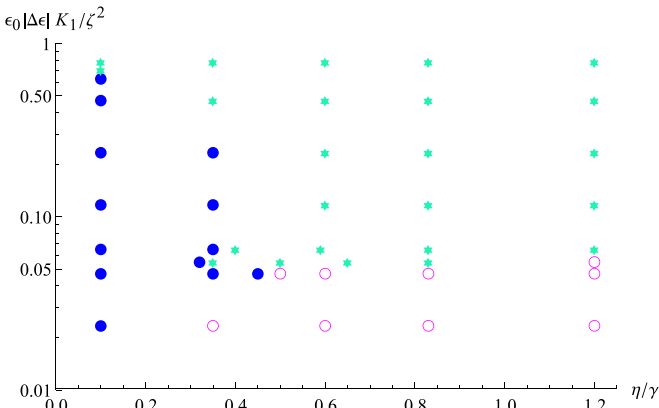
FIG. 5. The phase diagram of instabilities at different η for the harmonic external field. Designations: $*$ is the phase with $q_x = 0$ and real Λ, $\circ$ is the phase with $q_x \neq 0$ and real Λ, and $\bullet$ is the phase with $q_x \neq 0$ and complex Λ
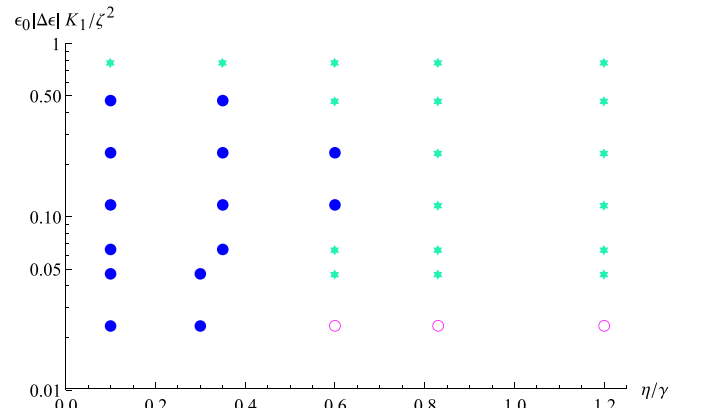
FIG. 6. The phase diagram of instabilities at different η and ζ for the pulsing external field. Designations: $*$ is the phase with $q_x = 0$ and real Λ, $\circ$ is the phase with $q_x \neq 0$ and real Λ, and $\bullet$ is the phase with $q_x \neq 0$ and complex Λ.
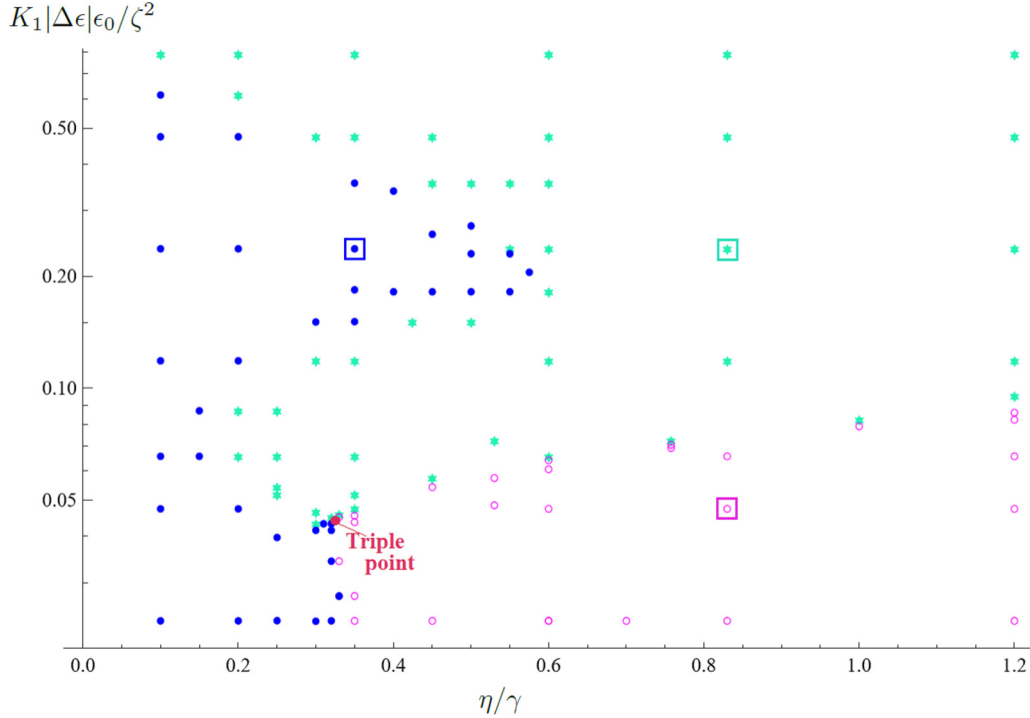
FIG. 7. The phase diagram of instabilities at different η and ζ for harmonic external field and different Frank modules $K_1 = 7 \times 10^{-12}$ N, $K_2 = K_3 = 5 \times 10^{-12}$ N, and under other parameters values: $q_z = 0.41$ µm^{-1}, $\sigma_\perp = 10$ s$^{-1} = 10^{-9}$ Ω^{-1} m^{-1}, $\Delta\sigma = -2$ s$^{-1} = 0.2 \times 10^{-9}$ Ω^{-1} m^{-1}, $\epsilon_\perp = 14$, $\Delta\epsilon = -3$, $\gamma = 0.066$ Pa s, $\omega = 2\pi \times 500$ s^{-1}. Designations: $*$ is the phase with $q_x = 0$ and real Λ, $\circ$ is the phase with $q_x \neq 0$ and real Λ, and $\bullet$ is the phase with $q_x \neq 0$ and complex Λ.

coefficients) is true also for the dynamic flexoelectric instability we are interested in our work. Thus we provided calculations of the critical electric-field amplitude as a function of the Frank-constant ratio K_2/K_1. Doing so for the typical for NLC inequality $K_2 < K_1$ we obtain the dependence that coincides with the results of Refs. [8,12], the critical electric field amplitude increases as the ratio K_2/K_1 increases up to unity. The results are presented in Fig. 8.
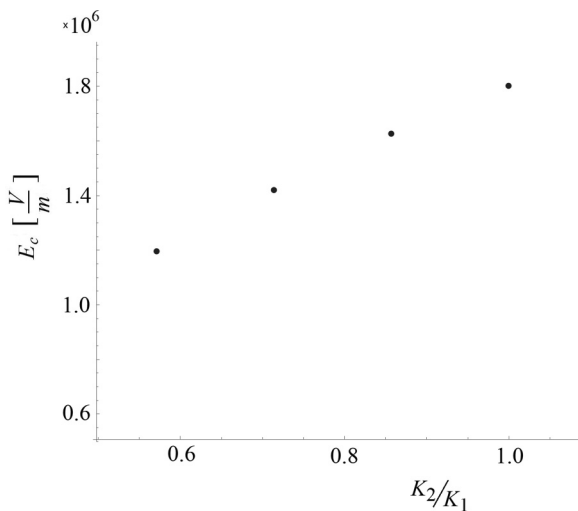
FIG. 8. Critical electric-field amplitude E_c as a function of Frank constants ratio K_2/K_1, for the certain material parameters for the case considered in Table III.

Let note, that the imaginary part of the amplification factor weakly depends on the electric field and on its frequency in the vicinity of the threshold. The nonzero imaginary part of the amplification factor appears as a result of hybridization of two modes and can exist at any absolute value of the amplification factor. The conclusion is confirmed by our computations. Typical examples presenting the behavior of the imaginary part of the amplification factor and its absolute value as functions of the electric-field amplitude are given in Fig. 9, which illustrates our conclusions for the certain set of the material parameters. We found that the results for the periodic boundary conditions and for the realistic set of boundary conditions (19) are close.

In addition, we examined the extended model with three different Frank moduli and with two different flexocoefficients for some sets of other material parameters and found that the behavior near the instability threshold is qualitatively the same as for the simplified model, see Figs. 1, 3, 5, 6, 10. Our results for the extended model are presented in Figs. 2–4, 7, 11, and 12 for the periodic boundary conditions and can be found also in Appendix B for a film with the realistic boundary conditions. We have also investigated the extended model with two flexo-coefficients. It gives qualitatively the same results.

B. Transitions between the regimes

The aim of this section is to add a bit more details about transitions between the different regimes of the instability. On the phase diagrams the transitions are reflected as the borders between regions with different character of the instability.
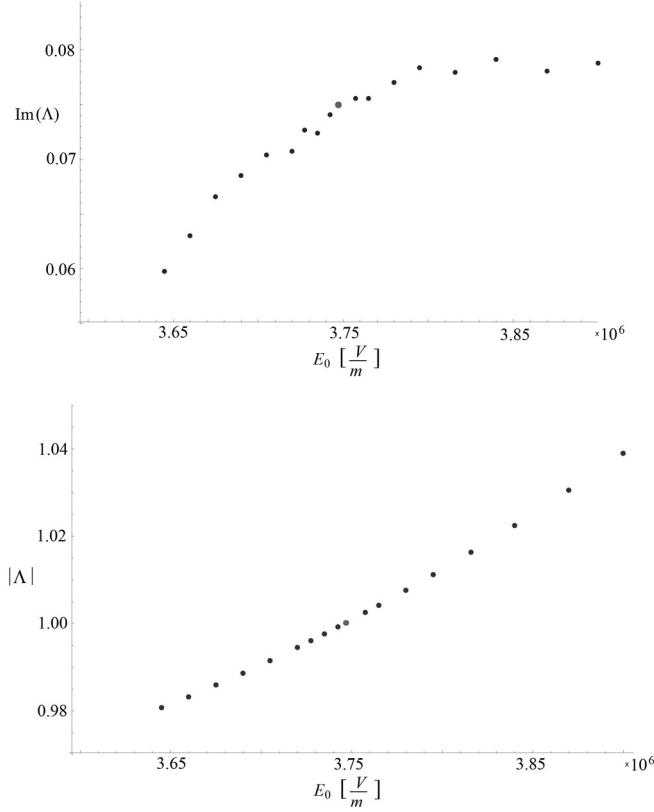
FIG. 9. Typical dependencies of square of Im(Λ) and $|\Lambda|$ on the amplitude of the electric field, respectively, for the certain material parameters for the case considered in Table I.

The transitions between the different regimes, which (depending of the material parameters) can be continuous (soft bifurcation) or jump-like (hard bifurcation). For example the transition from the case $q_x = 0$, real Λ to the case $q_x \neq 0$, complex Λ occurs discontinuously (with a jump from one type of the critical mode to another one), see Fig. 10. In turn, the transition from the case $q_x \neq 0$, real Λ to the case $q_x \neq 0$, complex Λ occurs continuously, see Fig. 11. In particular, Fig. 11 demonstrates how the maximum with complex Λ appears at the transition from two-dimensional pattern regime with real Λ, to the oscillating regime. The transition occurs continuously at the varying dimensionless parameter η/γ.

As it concerns the transition from the case $q_x = 0$, real Λ to the case $q_x \neq 0$, real Λ, it can be either continuous or with a jump between the competing critical modes, depending on the material parameters. The continuous transition can be easily realized for the case of different Frank modules. This case is illustrated in Fig. 12, corresponding to the continuous transition from the static stripes regime to the two-dimensional director pattern regime upon variation of the parameter η/γ.

It is instructive to examine in more details the transition to the oscillating regime from the stationary stripe structure. The transition occurs by the variations of the parameters listed in (12). Near the transition a competition of potentially critical modes takes place. Typically, the modes with the complex amplification factor Λ, having maximum at $q_x \neq 0$, $q_y \neq 0$, compete with the mode with the real amplification factor Λ, which has the maximum at $q_x = 0$, $q_y \neq 0$. The transition

takes place when the absolute values of the amplification factors of both modes are equal to unity, thus it is a discontinuous transition. To illustrate the phenomenon, we present the computation results demonstrating the transition to the oscillating regime from the regime of stationary stripes under

$$\eta/\gamma = 1, \quad \Delta\epsilon/\epsilon_\perp = -0.07 \div -0.052,$$

$$K_1|\Delta\epsilon|\epsilon_0/\zeta^2 = 0.095,$$

in Fig. 10. The transition occurs at varying (decrease) $|\Delta\epsilon|/\epsilon_\perp$. The complete set of the parameters used for the computations is presented in the caption to Fig. 10.

Note that our calculations confirm that the instability (with the finite wave vectors) is also possible only if $\zeta^2 > C|\Delta\epsilon|K$, with certain values of C in accordance with the criterion (11), as discussed above.

We studied numerically the dependencies of the critical electric field E_c and of the critical wave vector on the frequency ω. We confirmed that the estimates (9) and (10) are valid. We provide the typical examples of the discussed dependencies in Figs. 13 and 14, which correspond to (9) and (10) for certain sets of the material parameters given in Table I.

V. REALISTIC BOUNDARY CONDITIONS

Here we consider the case of the realistic boundary conditions (19). Computations of the dynamic flexoelectric instability for such case are more involved and computer time consuming than for case of periodic boundary conditions. The complete system of the linear equations describing the nematic dynamics is the system of six equations (13)–(18). All the equations are of the second order in ∂_z. In addition to the equations, one should use the boundary conditions (19) at the surfaces of the film.

It is convenient to exclude the "pressure" Π from the system of equations, thus reducing the number of the equations to five. Of course, the order of the equations after the exclusion is increased. It is possible to obtain an equation of the fourth order for v_z, keeping the orders of the equations for other variables to be equal to two. The system of such equations ideally corresponds to the boundary conditions (19). Let us sketch a derivation of the equations.

To find the equation for v_z, one applies $\partial_z^2 - q^2$ to Eq. (16) and then expresses $(\partial_z^2 - q^2)\Pi$ from Eq. (18) to obtain

$$\rho(\partial_z^2 - q^2)\partial_t v_z = \eta(\partial_z^2 - q^2)^2 v_z - i\zeta E(t)q_x^3 \partial_z n_z - \zeta q_x^4 \partial_z \Phi$$
$$- K(\partial_z^2 - q^2)q_x(\partial_z q_y n_y - iq^2 n_z)$$
$$+ \epsilon_\perp \epsilon_0 E(t)q^2(\partial_z^2 - q^2)\Phi. \quad (25)$$

Next, applying ∂_z to Eq. (16) and expressing then $\partial_z^2\Pi$ from Eq. (18), one finds

$$q^2\Pi = -\rho\partial_t\partial_z v_z + \eta(\partial_z^2 - q^2)\partial_z v_z$$
$$- i\zeta E q_x^3 n_z - \zeta q_x^4 \Phi - K(\partial_z^2 - q^2)q_x q_y n_y. \quad (26)$$

Substituting the expression into Eq. (15), we find the equation for v_y. There is the term proportional to $\partial_z^3 n_y$ in Eq. (25). Applying ∂_z to Eq. (13) we can then express $\partial_z^3 n_y$, then substituting it into Eq. (25). In more detail, the derivation and the
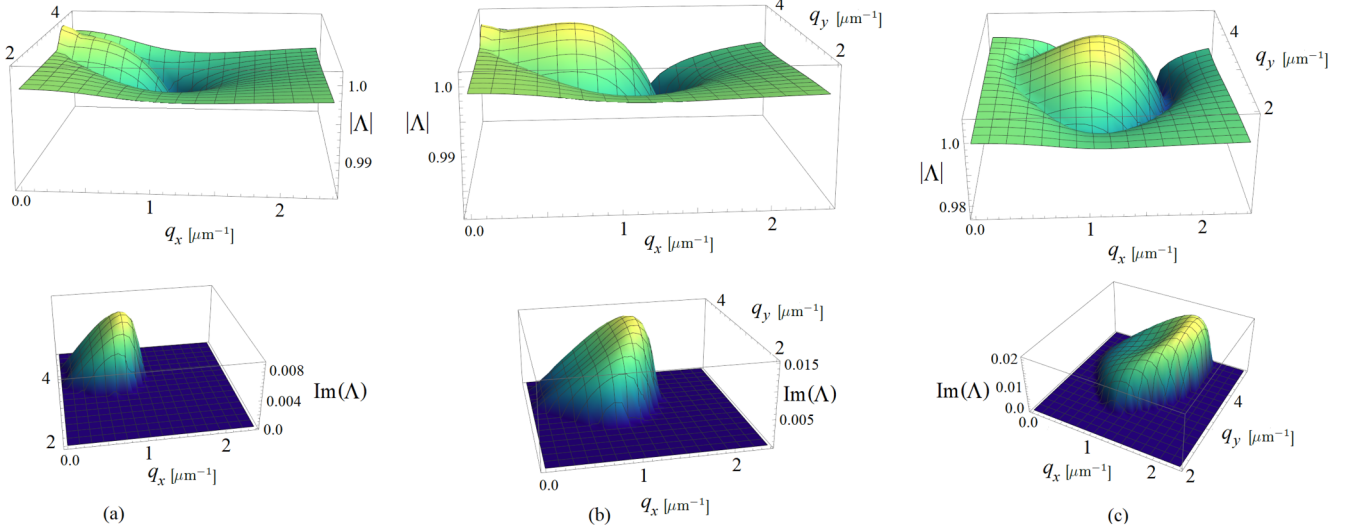
FIG. 10. Change of principal modes spectrum $|\Lambda|$ under transition from static strips regime to oscillating regime: (a) $\epsilon_\perp = 18$ and $\Delta\epsilon/\epsilon_\perp = -0.07$; (b) $\epsilon_\perp = 19.4$ and $\Delta\epsilon/\epsilon_\perp = -0.065$; (c) $\epsilon_\perp = 24$ and $\Delta\epsilon/\epsilon_\perp = -0.052$ and other parameters: $\omega = 2\pi \times 500$ s^{-1}, $E_{bc} = 3.94 \times 10^6$ V/m, $q_z = 0.41$ μm^{-1}, $\sigma_\perp = 1$ s$^{-1} = 10^{-10}$ Ω^{-1} m^{-1}, $\Delta\sigma = -0.2\sigma_\perp$, $K = 4 \times 10^{-12}$ N, $\zeta = (6.5/3) \times 10^{-11}$ C m^{-1}, $\Delta\epsilon = -4\pi \times 10^{-1}$, $\gamma = 0.06$ Pa s, $\eta = 0.06$ Pa s.

resulting equations are presented in Appendix A, Eqs. (A20) and (A21).

One can check, that after substitution (cf. with Ref. [37])

$$v_x \rightarrow -iv_x, \quad v_y \rightarrow -iv_y, \quad n_z \rightarrow -in_z, \quad (27)$$

to the equations we arrive at the system of equations with real coefficients for the new variables.

In the framework of our computational scheme, we solve the Cauchy problem for the system of differential equa-

tions for the fields $u_\alpha(z) = (n_y, n_z, v_y, v_z, \Phi)$, starting from some initial condition at $t = 0$ and satisfying the boundary conditions (19). The problem is solved numerically for a period of the external electric field or for a number of periods.

To examine the instability, we use the scheme based on approximating the functions u_α by an expansion over a finite basis. Namely, we chose a set of N_f basic functions $g_{\alpha,j}(z)$ where the first subscript, $\alpha = 1 \div 5$ corresponds to the
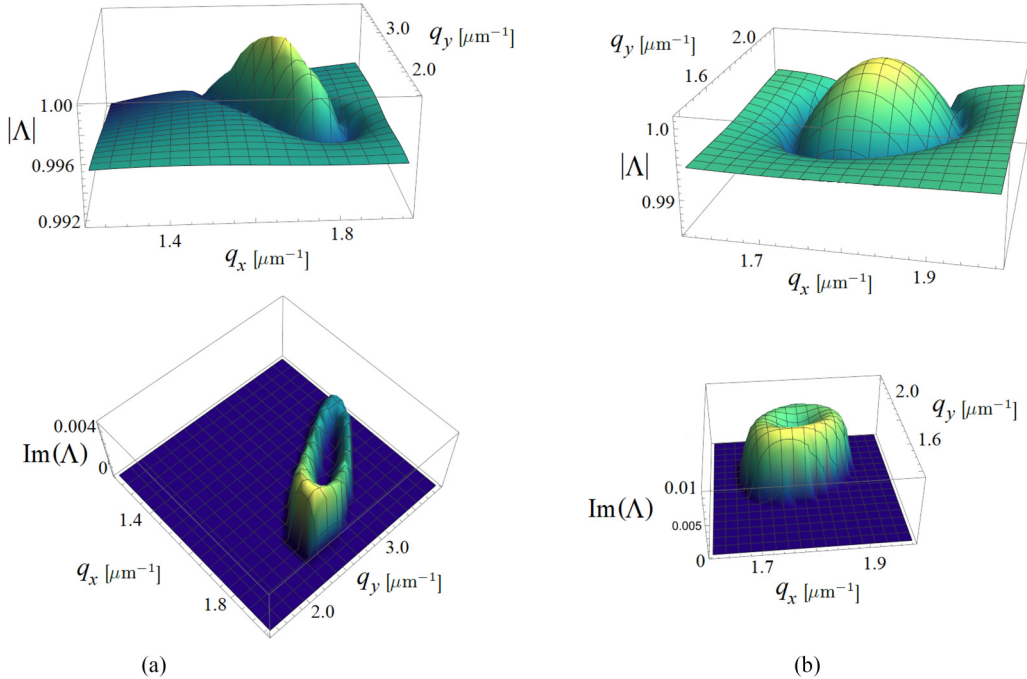
FIG. 11. Change of principal modes spectrum $|\Lambda|$ under transition from two-dimensional director pattern regime maximum with real Λ to oscillating regime: (a) $\eta/\gamma = 0.35/0.66$ and $E_{bc} = 0.93 \times 10^6$ V/m; (b) $\eta/\gamma = 0.25/0.66$ and $E_{bc} = 0.9 \times 10^6$ V/m; and other parameters: $\omega = 2\pi \times 500$ s^{-1}, $q_z = 0.4$ μm^{-1}, $\sigma_\perp = 10$ s$^{-1} = 10^{-9}$ Ω^{-1} m^{-1}, $\Delta\sigma = -0.2\sigma_\perp$, $K_1 = 7 \times 10^{-12}$ N, $K_2 = 5 \times 10^{-12}$ N, $K_3 = 5 \times 10^{-12}$ N, $\zeta = (26.46/3) \times 10^{-11}$ C m^{-1}, $\epsilon_\perp = 14$, $\Delta\epsilon = -0.75$, $\gamma = 0.066$ Pa s.
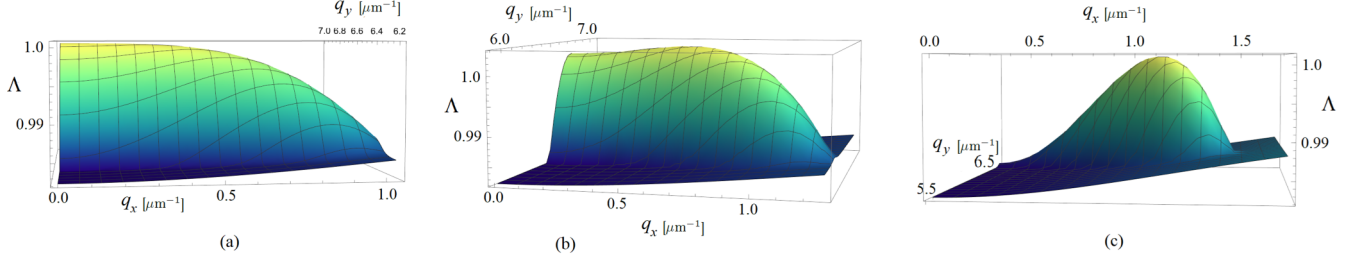
FIG. 12. Transition from the static stripes regime to two-dimensional director pattern one with amplification factor maximum position: (a) $q_x = 0$, $q_y = 6.68\ \mu\text{m}^{-1}$, $\eta/\gamma = 0.5/0.66 = 0.76$; (b) $q_x = 0.66\ \mu\text{m}^{-1}$, $q_y = 6.55\ \mu\text{m}^{-1}$, $\eta/\gamma = 0.54/0.66 = 0.82$; (c) $q_x = 1\ \mu\text{m}^{-1}$, $q_y = 6.3\ \mu\text{m}^{-1}$, $\eta/\gamma = 1$. Dependencies of amplification factor Λ of the principal mode on q_x, q_y at $\omega = 2\pi \times 500\ \text{s}^{-1}$, $E_{bc} \simeq 1.86 \times 10^6$ V/m for $q_z = 0.41\ \mu\text{m}^{-1}$, $\sigma_\perp = 10\ \text{s}^{-1} = 10^{-9}\ \Omega^{-1}\,\text{m}^{-1}$, $\Delta\sigma = -0.2\sigma_\perp$, $K_1 = 7 \times 10^{-12}$ N, $K_2 = 5 \times 10^{-12}$ N, $K_3 = 5 \times 10^{-12}$ N, $\zeta = (15.6/3) \times 10^{-11}$ C m^{-1}, $\epsilon_\perp = 14$, $\Delta\epsilon = -3$, $\gamma = 0.066$ Pa s.

fields n_y, n_z, v_y, v_z, Φ and the second subscript $j = 1 \div N_f$ numerates the functions of the set. Thus we arrive at the expansion

$$u_\alpha(z) = \sum_{j=1}^{N_f} f_{\alpha,j} g_{\alpha,j}(z), \tag{28}$$

where $f_{\alpha,j}$ are some coefficients.

To guarantee the correct boundary conditions for the fields n_y, n_z, v_y, v_z, Φ the appropriate boundary conditions should be imposed on the basis functions $g_{\alpha,j}(z)$. Namely, the functions $g_{\alpha,j}$ should be zero at $z = \pm d/2$. In addition, the functions $g_{4,j}$, figuring in the expansion of v_z, should have zero z derivatives at $z = \pm d/2$, see Eq. (19). We use the following basic set of the functions. For the fields n_y, n_z, v_y, and Φ we use the sinusoidal basic functions

$$g_{\alpha,j}(z) = \sin\left[\pi j(z/d + 1/2)\right], \quad \alpha = 1, 2, 3, 5,$$
$$j = 1, \ldots, N_f; \tag{29}$$

equal to zero at $z = \pm d/2$. For the field v_z we choose the basic functions

$$g_{4,j}(z) = (z^2 - d^2/4)\sin\left[\pi j(z/d + 1/2)\right], \quad j = 1, \ldots N_f; \tag{30}$$

satisfying both boundary conditions, $v_z = 0$ and $\partial_z v_z = 0$.

To pass from the fields $u_\alpha(z)$ to the coefficients $f_{\alpha,j}$ one should define the projection procedure $u \to f$. For the purpose we use the metrics L_2, which corresponds to the usual notion of distance between points in the plane, then

$$f_{\alpha,a} = \sum_b M^{-1}_{\alpha,ab} \int dz\, g_{\alpha,b}(z) u_\alpha(z). \tag{31}$$

The matrices $\hat{M}_\alpha$ in Eq. (31) are five matrices $N_f \times N_f$ with the components

$$M_{\alpha,ab} = \int dz\, g_{\alpha,a}(z) g_{\alpha,b}(z). \tag{32}$$

The matrices $\hat{M}_\alpha$ are, obviously, symmetric.

After solving Cauchy problem on one period and projecting the initial and the final values of the fields u_α in accordance with Eq. (31), we find the coefficients $f_{\alpha,j}(0)$ and $f_{\alpha,j}(T)$. The linear character of our problem means that

$$f_{\alpha,a}(T) = \sum_{\beta,b} W_{\alpha,a;\beta,b} f_{\beta,b}(0). \tag{33}$$

The matrix $\hat{W}$ is a $5N_f \times 5N_f$ matrix, which represents a generalization of the matrix 5×5 figuring in Eq. (23). We call the matrix $\hat{W}$ the evolution matrix as well. Eigenvalues Λ_i of the evolution matrix $\hat{W}$ determine the amplification factors

FIG. 13. Dependence of square of the critical electric field E_c^2 on the frequency for the certain other material parameters for the case considered in Table I. The calculated values of E_c^2 are represented by points, and linear fit by thin solid line, respectively.
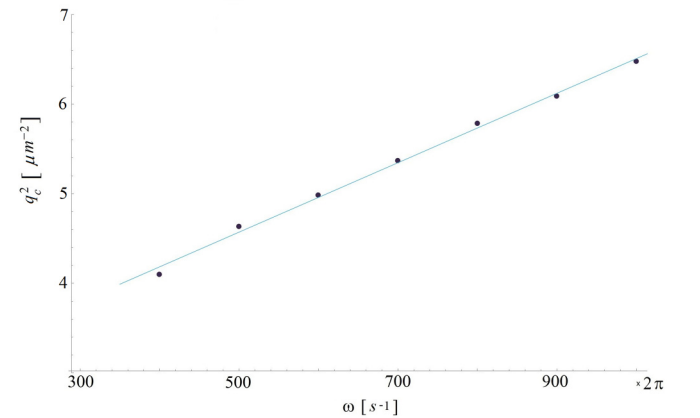
FIG. 14. Dependence of square of critical wave vector $q_c^2 = q_{cx}^2 + q_{cy}^2 + q_{cz}^2$ on the frequency for the certain other material parameters for the case considered in Table I. The calculated values of q_c^2 are represented by points, and linear fit by thin solid line, respectively.
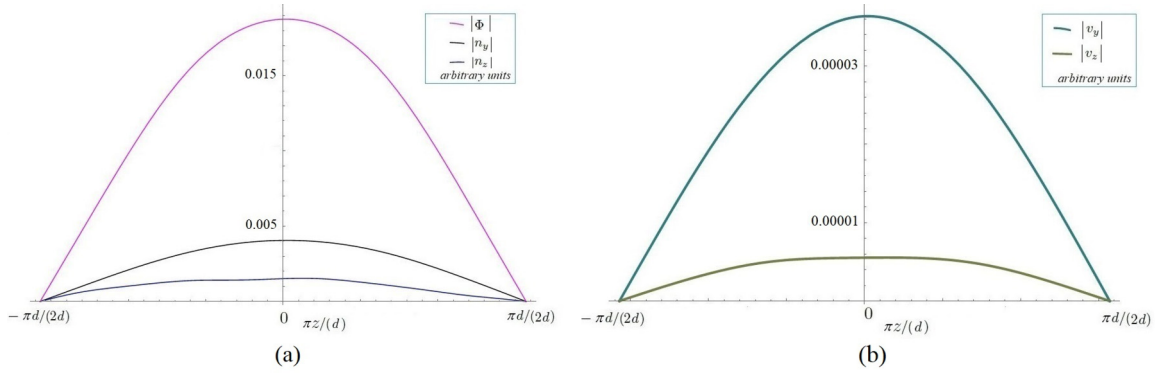
FIG. 15. Principal eigenmodes for (a) the fields n_y, n_z, Φ and (b) for the fields v_y, v_z as functions of $\pi z/d$, for $t = 150T$.

of the eigenmodes during the period T and, consequently, the characteristic exponents via the relations $\Lambda_i = \exp(\lambda_i T)$. Since after the substitution (27) we deal with the differential equations with real coefficients, the amplification factors Λ_i or the characteristic exponents λ_i are all real or, in addition to the real parameters, there are pairs of complex conjugated parameters.

The evolution matrix $\hat{W}$ can be found, if we subsequently solve Cauchy problem for the set of the initial functions $g_{\alpha,a}(z)$ at $t = 0$. Expanding the resulting functions at $t = T$ in accordance with the rule (31), we find the set of the coefficients $W_{\alpha,a;\beta,b}$ constituting the evolution matrix $\hat{W}$, determining the evolution of the system during the period. Ultimately, we are interested in the eigenfunctions of the evolution matrix $\hat{W}$ and in the corresponding eigenvalues Λ. More precisely, we are interested in the eigenfunction with the principal Λ (that is with maximal $|\Lambda|$), since just the eigenfunction describes the instability.

Luckily it turns out that, for the critical mode, the amplitudes at the basis functions g_j in the eigenfunction expansion decay sufficiently fast with its number with the use of a reasonable set of the basis functions. The values of the amplification factors Λ obtained for different numbers N_f of the basis functions converge as N_f increases. This fact verifies the regular convergence of the computational procedure. Thus, the described procedure allows one to obtain rather accurate quantitative description of the modes for the finite-thickness nematic film.

We established that, with the accuracy needed for this work, it is enough to take six basic functions, $N_f = 6$. Then the matrix $\hat{W}$ is a matrix 30×30, where 30 is the product of the number of the fields (five) and the number of basic functions ($N_f = 6$). It is not very easy to compute all eigenvalues of the matrix 30×30. However, we are interested solely in the principal mode. Therefore one can take the evolution during many (say N) periods. Then the eigenvalues of the corresponding evolution matrix are Λ^N. This trick essentially simplifies investigation of the principal mode.

The principal eigenmodes near the threshold found as a result of the described procedure for a certain set of the material parameters are plotted in Fig. 15. The behavior of the eigenfunctions is fairly smooth.

To justify explicitly that the results for the periodic boundary conditions and for the film of finite thickness under realistic boundary conditions (19) are close, we have performed the computations for both cases with the identical sets of the material parameters. As an illustration, we have chosen three sets of the material parameters corresponding to all three types of the flexoelectric instability. They correspond to the points marked by squares on the phase diagram in Fig. 7. The results are summarized in the tables given in Appendix B. In the tables we show the values of the critical electric field and the values of the amplification factor Λ in the vicinity of the critical wave vector. The results confirm our expectations.

Note that when we investigate phase behavior of the system over varying film thickness d only, under fixed other material parameters, starting from oscillating regime, we always go upon decreasing of d to stationary stripe regime (trivial maximum with $q_x = 0$).

VI. CONCLUSION

In this work we find that the flexoelectric instability of NLCs in the external alternating electric field can lead to different inhomogeneous spatio-temporal structures of the director field $\boldsymbol{n}$ if a certain threshold value of the field is exceeded. The subject of our consideration are nematics with negative anisotropy of both the dielectric permittivity $\epsilon_\parallel - \epsilon_\perp < 0$ and the conductivity $\sigma_\parallel - \sigma_\perp < 0$, whereas above the subscripts $\parallel$ and $\perp$ designate the components along the director $\boldsymbol{n}$ and perpendicular to it. We analyzed the nematic film placed between two parallel conducting plates with the alternating electric potential differences applied to the plates. Then the electric field $\boldsymbol{E}$, directed perpendicular to the plates, is induced inside the film. Below the transition the state is assumed to be homogeneous with the director oriented along the surfaces of the plates. Such ordering is caused by suitable boundary conditions for the director at the surfaces.

We study numerically the flexoelectric instability based on the linearized dynamic equations of nematics. The set of the equations cannot be solved analytically in the external alternating electric field. To find the qualitative peculiarities of the flexoelectric instability, we studied first the case when the boundary conditions can be ignored. Therefore, after Fourier transform all the fields have harmonic dependence with a wave vector q_z in the direction perpendicular to the plates. Then the equations can be easily solved numerically. To check whether such approach is physically adequate, we performed

much more involved computations for the nematic films of finite thickness for the planar boundary conditions for the director, no slipping boundary conditions for the hydrodynamic velocity and fixing the electric potential at the plates. We show that the results for both cases are close to each other if we choose $q_z = \pi/d$, where d is the thickness of the film. This slightly surprising finding can be crudely understood by the fact that for Fourier harmonics relevant for the instability characteristic space scale along the z axis is smaller than that in the orthogonal plane. We obtained that for, the case of sufficiently thick film, the results for the periodic boundary conditions and for the case of realistic boundary conditions (19) are close.

The flexoelectric instability is related to the distortions of the director field. However, in dynamics the director is coupled to hydrodynamic and electromagnetic degrees of freedom, that leads to a complicated structure of the critical mode, becoming unstable at increasing the external electric field. If the excitation with $q_x = 0$ and $q_y \neq 0$ becomes unstable first then a stationary stripe structure appears above the threshold. This scenario is well known and described in the literature. If the both components $q_x \neq 0$ and $q_y \neq 0$ then the state above the threshold is determined by nonlinear terms. Both oblique rolls or various two-dimensional periodic structures could be realized above the threshold.

We revealed the third possibility (somehow overlooked in the previous works), the mode with the tilted wave vector and with the complex characteristic exponent of the critical mode. Then nonstationary (oscillating in time) structures appear above the threshold. They are propagating or standing waves. We demonstrate numerically that the scenario with the oscillating structures can take place at a set of parameters for the computations for both cases of boundary conditions: periodic and realistic (19).

We show that the third scenario is realized at the condition (7), leading to the existence of a slowly decaying "potential" mode describing the relaxation of the electric-field fluctuations. Then in a range of the wave vectors q_x and q_y the hybridization occurs of the "potential" mode and of the "soft director" mode related to the director instability. The hybridization could lead to the instability characterized by a complex characteristic exponent λ that determines the behavior $\propto \exp(\lambda t)$ of the critical mode for times larger than the period. In the case λ is purely imaginary at the threshold. Note that the scenario needs that the both components of the lateral wave vector of the critical mode be nonzero ($q_x \neq 0$ and $q_y \neq 0$).

We are confident in our main physical result (oscillating in time patterns). The accuracy of our computation of the magnitude of Λ can be estimated as the limiting numerical calculation error, which is of the order of 1×10^{-8} for float values (and 1×10^{-15} for double values, which were used in some simulations). To justify that our results are correct and sufficiently robust, we developed and used different algorithms for calculation of Λ. We used the sinusoidal and the pulse external electric field, and we utilized the periodic and the realistic boundary conditions. The results for the cases are close.

The condition (7) is crucial for our scenario. It can be achieved, e.g., in purified from impurities NLCs (for this point, see the discussion of this issue in Refs. [28–30]). Let us stress that the obligatory ingredient for the third scenario is the coupling of director to hydrodynamic degrees of freedom (neglecting hydrodynamic velocity $\boldsymbol{v}$ and its fluctuations makes the third scenario impossible). Our computations show also that the dielectric anisotropy of the nematic should be relatively weak for the realization of the third scenario. The condition can be satisfied for NLCs near the transition temperature to the isotropic phase (or for the alternating field frequency in the vicinity of the so-called inversion point, where the dielectric anisotropy changes its sign).

It is worth noting that, upon decreasing the film thickness d (keeping all other parameters fixed), we always find the transition from the oscillating-in-time two dimensional patterns into the stationary stripe regime (with $q_x = 0$). The oscillating-in-time patterns can be realized for the relatively thick films. Quantitatively, it implies the condition $qd \gtrsim 1$, where the characteristic wave vector q of the unstable harmonic is determined by Eq. (9).

We examined mainly the case of the external electric field harmonically varying with time. One can consider another possibility of the external alternating electric field. Namely, the field can be the pulse function (telegraph process). Then the system of equations for the case of periodic boundary conditions can be solved practically up to the end without numerical computations. We show that the results derived in the framework of this model are similar to those for the sinusoidal field. In particular, the oscillating-in-time or propagating patterns are realized for some region of parameters near the threshold field. The results confirm the universal character of our findings.

In our work we performed a linear stability analysis of NLC films in an external alternating electric field for sufficiently small electric conductivity. Unfortunately, we did not find in the literature any experimental results satisfying the necessary condition of applicability (7) of our dynamic theory: $\omega \gg D/r_D^2$, which can be rewritten as $\omega \gg \sigma/(\epsilon_0 \epsilon_\perp)$. For instance, the results provided in Ref. [37] are obtained for values of conductivities and electric-field frequencies that do not satisfy the condition (7). Scanning the literature we did not find experimental evidence for our main theoretical result: the prediction of oscillating-in-time two-dimensional patterns. We hope that the direction of search suggested by our analysis in terms of the parameters (12) and applicability conditions (7), (10), and (11) enables one to find a suitable materials where this type of the instability will be observed. The phase diagrams presented in our work can be useful for search of materials where oscillating-in-time $2d$ structures will be observed.

We should admit that there are some physical ingredients missed in our approach. Note, as an example, the external, injected from electrodes charges, leading to the local violation of the electroneutrality [40]. Note to the point that a finite electric current limits the overall thermalization of the NLCs, and in such that the instantaneous values of the material parameters can additionally be position-dependent across the sample. Another missing in our publication ingredient is the possible nonuniformity of the director surface anchoring. This ingredient has been introduced recently [55,56] to simulate numerically localized and propagating

excitations in the NLCs. However in this works the hydrodynamic degrees of freedom and finite conductivity were disregarded. Keeping everything said above in mind, we should admit that further theoretical and experimental work is required before a full understanding of dynamical flexoelectric instability in NLCs is reached. Nevertheless we do believe that the physics behind our simplified model has to be understood before adding the additional ingredients. The same concerns nonlinear effects. The solution of the nonlinear dynamic equations is needed to identify the structure above the threshold. The analysis is a subject of future works.

ACKNOWLEDGMENTS

APPENDIX A: TECHNICAL DETAILS OF CALCULATIONS

First of all, let us note that the equations following from Eqs. (13)–(17) for the periodic BC case are written as

$$\partial_t n_y = iq_x v_y + \frac{1}{\gamma}[-Kk^2 n_y - i\zeta q_y n_z E - \zeta q_x q_y \Phi], \quad \text{(A1)}$$

$$\partial_t n_z = iq_x v_z + \frac{1}{\gamma}[-Kk^2 n_z + i\zeta q_y n_y E + \epsilon_0 \Delta\epsilon E^2 n_z$$
$$- i\epsilon_0 \Delta\epsilon E q_x \Phi - \zeta q_x q_z \Phi], \quad \text{(A2)}$$

$$\rho\partial_t v_y = -\eta k^2 v_y - iq_y \Pi + iKk^2 q_x n_y, \quad \text{(A3)}$$

$$\rho\partial_t v_z = -\eta k^2 v_z - iq_z \Pi + iKk^2 q_x n_z - \epsilon_0 \epsilon_\perp E k^2 \Phi, \quad \text{(A4)}$$

$$- \partial_t\big[-\epsilon_0\epsilon_\parallel q_x^2 \Phi - \epsilon_0\epsilon_\perp\big(q_y^2 + q_z^2\big)\Phi$$
$$+ iq_x(\epsilon_0\Delta\epsilon n_z E + i\zeta q_y n_y + i\zeta q_z n_z)\big]$$
$$= -\sigma_\parallel q_x^2 \Phi - \sigma_\perp\big(q_y^2 + q_z^2\big)\Phi + i\Delta\sigma E q_x n_z, \quad \text{(A5)}$$

where solutions of the system (13)–(17) are proportional to $\exp(iq_z z)$, and $k^2 = q^2 + q_z^2 = q_x^2 + q_y^2 + q_z^2$. In this case the "pressure" Π figuring in the equations is expressed as

$$-\Pi = i\zeta E q_x^3 n_z/k^2 + \zeta q_x^4 \Phi/k^2 - Kq_x(q_y n_y + q_z n_z)$$
$$+ i\epsilon_0\epsilon_\perp E q_z \Phi, \quad \text{(A6)}$$

as a consequence of Eq. (18).

In the next step let discuss the technical details for realistic boundary conditions Analyzing the uniform film it is convenient to make Fourier transform in terms of the longitudinal coordinates x and y. Doing so, one can rewrite Eq. (A5) in the

form

$$\partial_t\big[\epsilon_\parallel\epsilon_0 q_x^2 \Phi + \epsilon_\perp\epsilon_0\big(q_y^2 - \partial_z^2\big)\Phi\big]$$
$$+ q_x\partial_t[\Delta\epsilon\epsilon_0 E(t)in_z + \zeta(-q_y n_y + i\partial_z n_z)]$$
$$= -\sigma_\parallel q_x^2 \Phi + \sigma_\perp\big(-q_y^2 + \partial_z^2\big)\Phi - (\sigma_\parallel - \sigma_\perp)E(t)q_x in_z, \quad \text{(A7)}$$

in turn, equation for the "pressure" Π takes the form

$$\big(-q^2 + \partial_z^2\big)\Pi$$
$$= \zeta E(t)q_x^3 in_z + \zeta q_x^4 \Phi - K\big(-q^2 + \partial_z^2\big)q_x(-q_y n_y + i\partial_z n_z)$$
$$- \epsilon_\perp\epsilon_0 E(t)\partial_z\big(-q^2 + \partial_z^2\big)\Phi, \quad \text{(A8)}$$

where $q^2 = q_x^2 + q_y^2$. Equations for the velocity components can be rewritten as

$$\big[\rho\partial_t - \eta\big(-q^2 + \partial_z^2\big)\big]iv_x = q_x\Pi + \zeta E(t)q_x^2 in_z + \zeta q_x^3 \Phi, \quad \text{(A9)}$$

$$\big[\rho\partial_t - \eta\big(-q^2 + \partial_z^2\big)\big]iv_y = q_y\Pi + K\big(-q^2 + \partial_z^2\big)q_x n_y, \quad \text{(A10)}$$

$$\big[\rho\partial_t - \eta\big(-q^2 + \partial_z^2\big)\big]v_z$$
$$= -\partial_z\Pi - K\big(-q^2 + \partial_z^2\big)q_x in_z - \epsilon_\perp\epsilon_0 E(t)\big(-q^2 + \partial_z^2\big)\Phi, \quad \text{(A11)}$$

and equations for n_y, n_z take the form

$$\partial_t n_y = q_x iv_y + \gamma^{-1}\big[K\big(-q^2 + \partial_z^2\big)n_y - \zeta q_y in_z E(t) - \zeta q_x q_y \Phi\big], \quad \text{(A12)}$$

$$i\partial_t n_z = -q_x v_z + \gamma^{-1}\big[K\big(-q^2 + \partial_z^2\big)in_z - \zeta q_y n_y E(t)$$
$$+ \Delta\epsilon\epsilon_0 E(t)in_z + \Delta\epsilon\epsilon_0 E(t)q_x\Phi - \zeta q_x\partial_z\Phi\big]. \quad \text{(A13)}$$

Let us emphasize, that Eqs. (A7), (A9)–(A13) constitute the transformed complete set for Φ, v_y, v_z, n_y, n_z with Π as defined in Eq. (A8).

After Fourier and (27) transformations of the velocity equations we obtain

$$(\rho\partial_t - \eta\nabla^2)(q_y v_z + i\partial_z v_y) = q_y f_z + i\partial_z f_y,$$
$$(\rho\partial_t - \eta\nabla^2)(i\partial_z v_x + q_x v_z) = i\partial_z f_x + q_x f_z, \quad \text{(A14)}$$
$$(\rho\partial_t - \eta\nabla^2)(q_x iv_y - q_y iv_x) = iq_x f_y - iq_y f_x,$$

where transformations of $\boldsymbol{f}$ components have the following form:

$$f_x = -i\big[\zeta E(t)q_x^2 in_z + \zeta q_x^3 \Phi\big],$$
$$f_y = -i\big[Kq_x\big(-q^2 + \partial_z^2\big)n_y\big], \quad \text{(A15)}$$
$$f_z = Kq_x\big(q^2 - \partial_z^2\big)in_z + \epsilon_\perp\epsilon_0 E(t)\big(q^2 - \partial_z^2\big)\Phi.$$

Then using the continuity equation we can exclude v_x as

$$iv_x = -(q_y iv_y + \partial_z v_z)/q_x. \quad \text{(A16)}$$

TABLE I. Amplification factor of the critical mode $\Lambda(q_x, q_y)$ in the vicinity of the main maximum for the case of periodic boundary conditions and for the film of finite thickness under realistic BCs (19) (Realistic BC). The case of oscillatory two-dimensional director pattern at $\zeta = 2.79 \times 10^{-11}$ C m^{-1}, $\eta = 0.023$ Pa s.

E_0 (V μm^{-1})	(q_x, q_y) (μm^{-1}, μm^{-1})	Λ Periodic BC	$\|\Lambda\|$ Periodic BC	Λ Realistic BC	$\|\Lambda\|$ Realistic BC
	(0.99, 1.87)	$0.997 \pm i0.075$	1.00012	$1.00085 \pm i0.0789509$	1.00396
	(1.155, 1.98)	$0.993 \pm i0.088$	0.997	$0.997 \pm i0.092$	1.0014
	(0.924, 1.81)	$0.997 \pm i0.07$	0.9997	$1.0007 \pm i0.071$	1.0032
3.75	(0.924, 1.923)	$0.996 \pm i0.071$	0.998	$0.999 \pm i0.075$	1.00195
	(0.924, 2.036)	$0.992 \pm i0.072$	0.995	$0.996 \pm i0.0726$	0.9988
	(0.957, 1.753)	$0.997 \pm i0.0716$	0.9999	$1.0007 \pm i0.0746$	1.0035
	(0.957, 1.81)	$0.9975 \pm i0.0721$	1.0001	$1.0012 \pm i0.073$	1.0039
	(0.924, 1.75)	$0.9974 \pm i0.0693$	0.9998	$1.0012 \pm i0.073$	1.0039
	(1.12, 1.92)	$0.994 \pm i0.085$	0.998	$0.998 \pm i0.087$	1.002
	(1.12, 2.205)	$0.99 \pm i0.088$	0.994	$0.994 \pm i0.092$	0.998
	(0, 0.34)	0.982	0.982	0.982	0.982
	(0, 1.923)	0.982	0.982	0.982	0.982
	(1.55, 0.396)	0.981	0.981	0.985	0.985

Thus we arrive to the following system of the equations for the velocity components v_y and v_z:

$$\rho q^2 \partial_t v_z - \rho \partial_t \partial_z^2 v_z = \eta\left(-q^4 v_z + 2q^2 \partial_z^2 v_z - \partial_z^4 v_z\right) + q^2 f_z$$
$$+ iq_y \partial_z f_y + iq_x \partial_z f_x, \quad (A17)$$

$$iq^2 \rho \partial_t v_y = i\eta\left(-q^2 + \partial_z^2\right)q^2 v_y - q_y\left[\rho \partial_t - \eta\left(-q^2 + \partial_z^2\right)\right]\partial_z v_z$$
$$+ q_x(iq_x f_y - iq_y f_x). \quad (A18)$$

The third-order derivative of n_y over z appears from the term $\partial_z f_y$ in Eq. (A17). To exclude this term it is possible to express it from Eq. (A12) as

$$\gamma^{-1} K \partial_z^3 n_y = \partial_t \partial_z n_y - q_x \partial_z i v_y + \gamma^{-1} \partial_z$$
$$\times [Kq^2 n_y + \zeta q_y i n_z E(t) + \zeta q_x q_y \Phi] \quad (A19)$$

and to substitute the obtained expression in Eq. (A17). As a result, we obtain the following equations for v_y and v_z:

$$i\rho q^2 \partial_t v_y = i\eta\left(-q^2 + \partial_z^2\right)q^2 v_y$$
$$- q_y\left[\rho \partial_t - \eta\left(-q^2 + \partial_z^2\right)\right]\partial_z v_z$$
$$- \zeta q_x^3 q_y[E_0 \cos(2\pi\tau)i n_z + q_x \Phi]$$
$$+ K_2 q_x^3 \partial_z^2 n_y - q_x^3\left(K_1 q_y^2 + K_3 q_x^2\right)n_y$$
$$+ (K_1 - K_2)q_x^3 q_y i \partial_z n_z, \quad (A20)$$

$$\rho\left(q^2 - \partial_z^2\right)\partial_t v_z$$
$$= -\eta\left(q^2 - \partial_z^2\right)^2 v_z + q^2\left\{q_x\left(K_2 q_y^2 + K_3 q_x^2 - K_1 \partial_z^2\right)i n_z\right.$$
$$- q_x(K_1 - K_2)q_y \partial_z n_y + \epsilon_\perp \epsilon_0 E_0 \cos(2\pi\tau)\left(q^2 - \partial_z^2\right)\Phi\right\}$$
$$+ q_x\left\{\gamma q_y \partial_t \partial_z n_y + \zeta E_0 \cos(2\pi\tau)q^2 i \partial_z n_z\right.$$
$$+ \zeta q_x q^2 \partial_z \Phi - \gamma q_x q_y i \partial_z v_y\right\}, \quad (A21)$$

where we account for, with three different Frank moduli, we have to replace the nematic elasticity terms in all equations as

follows:

$$K\nabla^2 n_y \rightarrow \left(K_1 \partial_y^2 + K_2 \partial_z^2 + K_3 \partial_x^2\right)n_y + (K_1 - K_2)\partial_y \partial_z n_z, \quad (A22)$$

$$K\nabla^2 n_z \rightarrow \left(K_1 \partial_z^2 + K_2 \partial_y^2 + K_3 \partial_x^2\right)n_z + (K_1 - K_2)\partial_y \partial_z n_y. \quad (A23)$$

APPENDIX B: COMPARISON

Here we present the comparison of the computation results of the flexoelectric instability for the case of periodic boundary conditions (periodic BC) and for the film of finite thickness (as an illustrative example we chose $d = 7.62$ μm) under realistic boundary conditions (19). The wave vector q_z for the periodic BC approach was equal to $q_z = \pi/d$. These two cases have been studied with identical material parameters. The following parameters were the same in all calculations: $\omega = 2\pi \times 500$ s^{-1}, $\sigma_\perp = 10^{-9}$ Ω^{-1} m^{-1} (10 s^{-1}), $\Delta\sigma = -0.2\sigma_\perp$, $K_1 = 7$ pN, $K_2 = 5$ pN, $K_3 = 5$ pN, $\epsilon_\perp = 14$, $\Delta\epsilon = -3$, $\gamma = 0.066$ Pa s. Parameters ζ and η were different; the corresponding values are presented in the headers of the tables. The results presented in Tables I–III and were

TABLE II. Amplification factor of the critical mode $\Lambda(q_x, q_y)$ in the vicinity of the main maximum for the case of periodic boundary conditions (Periodic BC) and for the film of finite thickness under the realistic BC (19) (Realistic BC). The static stripes case at $\zeta = 2.79 \times 10^{-11}$ C m^{-1}, $\eta = 0.055$ Pa s.

E_0 (V μm^{-1})	(q_x, q_y) (μm^{-1}, μm^{-1})	Λ Periodic BC	Λ Realistic BC
	(0, 1.56)	1.00031	1.00022
	(0, 1.18)	0.995	0.995
	(0, 1.8)	0.998	0.998
4	(0.052, 1.84)	0.9965	0.9964
	(0.052, 1.39)	0.9987	0.9987
	(0.21, 1.53)	0.9905	0.9906
	(0.21, 1.84)	0.989	0.989

TABLE III. Amplification factor of the critical mode $\Lambda(q_x, q_y)$ in the vicinity of the main maximum for the case of periodic boundary conditions and for the film of finite thickness under realistic BCs (19) (Realistic BC). The case of static periodic two-dimensional director pattern at $\zeta \approx 6.23 \times 10^{-11}$ C m^{-1}, $\eta = 0.055$ Pa s.

E_0 (V μm^{-1})	(q_x, q_y) (μm^{-1}, μm^{-1})	Λ Periodic BC	Λ Realistic BC
	(1.53, 5.25)	1.0002	0.9993
	(1.51, 5.25)	0.9998	0.9986
	(1.52, 5.25)	1.00009	0.9991
4	(1.52, 5.27)	1.00014	0.999
	(1.53, 5.32)	0.9995	0.9982
	(1.544, 5.20)	0.9999	0.9988
	(1.544, 5.31)	0.9996	0.99865
	(1.56, 5.22)	1.0001	0.99915
	(1.56, 5.34)	0.9982	0.9971
	(1.76, 5.86)	0.99	0.9907

TABLE IV. Amplification factor of the critical mode $\Lambda(q_x, q_y)$ in the vicinity of the main maximum for the case of periodic boundary conditions and for the film of finite thickness under realistic BC (19) (Realistic BC). The case of static periodic two-dimensional director pattern for the solution for the film at $\zeta \approx 6.23 \times 10^{-11}$ C m^{-1}, $\eta = 0.055$ Pa s.

E_0 (V μm^{-1})	(q_x, q_y) (μm^{-1}, μm^{-1})	Λ Periodic BC	Λ Realistic BC
	(1.53, 5.25)	1.0002	1.0001
	(1.51, 5.25)	0.9998	0.9996
	(1.52, 5.25)	1.00009	0.9999
4	(1.52, 5.27)	1.00014	0.99997
	(1.53, 5.32)	0.9995	0.9994
	(1.544, 5.20)	0.9999	0.9998
	(1.544, 5.31)	0.9996	0.99955
	(1.56, 5.22)	1.0001	1.00008
	(1.56, 5.34)	0.9982	0.998
	(1.76, 5.86)	0.99	0.99

obtained at calculation during a period, whereas for Table IV calculation was done for 150 periods of external field.

The tables illustrate the correspondence between the results for the case of periodic boundary conditions and for the film

of finite thickness under realistic boundary conditions (19) for all possible types of the instability. The obtained practically perfect agreement is a result of the smallness of q_z in comparison with the lateral wave vector.

[1] R. Williams, J. Chem. Phys. **39**, 384 (1963).
[2] G. Heilmeier, L. A. Zanoni, and L. Barton, Proc. IEEE **56**, 1162 (1968).
[3] W. Helfrich, J. Chem. Phys. **51**, 4092 (1969).
[4] J. D. Margerum, H. S. Lim, P. O. Braatz, and A. M. Lackner, Mol. Cryst. Liq. Cryst. (1969-1991) **38**, 219 (1977).
[5] I. Rehberg, S. Rasenat, J. Fineberg, M. de la Torre Juarez, and V. Steinberg, Phys. Rev. Lett. **61**, 2449 (1988).
[6] G. Goren, I. Procaccia, S. Rasenat, and V. Steinberg, Phys. Rev. Lett. **63**, 1237 (1989).
[7] I. Rehberg, S. Rasenat, and V. Steinberg, Phys. Rev. Lett. **62**, 756 (1989).
[8] S. A. Pikin, *Structural Transformations in Liquid Crystals* (Gordon and Breach, New York, 1991).
[9] R. B. Meyer, Phys. Rev. Lett. **22**, 918 (1969).
[10] Yu. P. Bobylev and S. A. Pikin, JETP **45**, 195 (1977).
[11] M. I. Barnik, L. M. Blinov, A. N. Trufanov, and B. A. Umanski, J. Phys. (Paris) **39**, 417 (1978).
[12] Yu. P. Bobylev, V. G. Chigrinov, and S. A. Pikin, J. Phys. Coll. (France) **40**(C3), C3-331 (1979).
[13] S. A. Pikin and B. A. Umanskii, Crystallogr. Rep. **63**, 641 (2018).
[14] S. Rasenat, E. Braun, and V. Steinberg, Phys. Rev. A **43**, 5728 (1991).
[15] E. Braun, S. Rasenat, and V. Steinberg, Europhys. Lett. **15**, 597 (1991).
[16] W. Zimmermann, MRS Bull. **16**, 46 (1991).
[17] S. Chandrasekhar, *Liquid Crystals* (Cambridge University Press, New York, 1992).
[18] P. G. de Gennes and J. Prost, *The Physics of Liquid Crystals* (Clarendon Press, Oxford, 1993).

[19] L. M. Blinov and V. G. Chigrinov, *Electrooptic Effects in Liquid Crystals* (Springer, New York, 1994).
[20] *Pattern Formation in Liquid Crystals*, edited by A. Buka, and L. Kramer (Springer, New York, 1996).
[21] S. Kai, K.-I. Hayashi, and Y. Hidaka, J. Phys. Chem. **100**, 19007 (1996).
[22] M. Kleman and O. D. Lavrentovich, *Soft Matter Physics: An Introduction* (Springer, New York, Berlin, Heidelberg, 2003).
[23] P. Oswald and P. Pieranski, *Nematic and Cholesteric Liquid Crystals: Concepts and Physical Properties Illustrated by Experiments*, Liquid Crystals Book Series (Taylor and Francis, London, 2005).
[24] S.-Q. Zhou and G. Ahlers, Phys. Rev. E **74**, 046212 (2006).
[25] M. Cross and H. Greenside, *Pattern Formation and Dynamics in Nonequilibrium Systems* (Cambridge University Press, Cambridge, 2009).
[26] K. Takahashi and Y. Kimura, Phys. Rev. E **90**, 012502 (2014).
[27] A. Krekhov, B. Dressel, W. Pesch, V. Delev, and E. Batyrshin, Phys. Rev. E **92**, 062510 (2015).
[28] B.-X. Li, V. Borshch, R.-L. Xiao, S. Paladugu, T. Turiv, S. V. Shiyanovskii, and O. D. Lavrentovich, Nat. Commun. **9**, 2912 (2018).
[29] B.-X. Li, R.-L. Xiao, S. Paladugu, S. V. Shiyanovskii, and O. D. Lavrentovich, Nat. Commun. **10**, 3749 (2019).
[30] B.-X. Li, R.-L. Xiao, S. V. Shiyanovskii, and O. D. Lavrentovich, Phys. Rev. Res. **2**, 013178 (2020).
[31] Y. Shen and I. Dierking, Soft Matter **16**, 5325 (2020).
[32] Y. Shen and I. Dierking, Commun. Phys. **3**, 14 (2020).
[33] Y. Shen and I. Dierking, Mater. Adv. **2**, 4752 (2021).
[34] Y. Shen and I. Dierking, Phys. Rev. Appl. **15**, 054023 (2021).
[35] S. Aya and F. Araoka, Nat. Commun. **11**, 3248 (2020).

[36] E. Kochowska, S. Nemeth, G. Pelzl, and A. Buka, Phys. Rev. E **70**, 011711 (2004).

[37] A. Krekhov, W. Pesch, N. Eber, T. Toth-Katona, and A. Buka, Phys. Rev. E **77**, 021705 (2008).

[38] T. Toth-Katona, N. Eber, A. Buka, and A. Krekhov, Phys. Rev. E **78**, 036306 (2008).

[39] W. Pesch, A. Krekhov, N. Eber, and A. Buka, Phys. Rev. E **98**, 032702 (2018).

[40] A. Earls and M. C. Calderer, Liq. Cryst. **49**, 742 (2022).

[41] E. I. Kats and V. V. Lebedev, *Fluctuational Effects in the Dynamics of Liquid Crystals* (Springer-Verlag, New York, 1993).

[42] P. M. Chaikin and T. C. Lubensky, *Principles of Condensed Matter Physics* (Cambridge University Press, Cambridge, 2000).

[43] E. S. Pikina, A. R. Muratov, E. I. Kats, and V. V. Lebedev, JETP **137**, 114 (2023).

[44] G. Floquet, Ann. Sci. Ecole Norm. Sup. **12**, 47 (1883).

[45] N. P. Erugin, *Linear Systems of Ordinary Differential Equations with Periodic and Quasi-Periodic Coefficients* (Academic Press, New York, 1966).

[46] N. Eber, P. Salamon, and A. Buka, Liq. Cryst. Rev. **4**, 101 (2016).

[47] L. D. Landau and E. M. Lifshitz, *Electrodynamics of Continuous Media*, Volume 8 in Course of Theoretical Physics, 2nd ed. (Pergamon Press, London, 1984).

[48] W. H. Jeu, *Physical Properties of Liquid Crystalline Materials* (Gordon and Breach, New York, 1980).

[49] M. C. Cross and P. C. Hohenberg, Rev. Mod. Phys. **65**, 851 (1993).

[50] W. H. Press, S. A. Teukolsky, W. T. Vetterling, and B. P. Flannery, *Numerical Recipes in Fortran, The Art of Scientific Computing* (Cambridge University Press, New York, 1992).

[51] E. I. Kats, Phys. Rev. E **103**, 012704 (2021).

[52] H. Nishikawa, K. Shiroshita, H. Higuchi, Y. Okumura, Y. Haseba, S. Yamamoto, K. Sago, and H. Kikuchi, Adv. Mater. **29**, 1702354 (2017).

[53] A. Mertelj, L. Cmok, N. Sebastián, R. J. Mandle, R. R. Parker, A. C. Whitwood, J. W. Goodby, and M. Copic, Phys. Rev. X **8**, 041025 (2018).

[54] N. Sebastian, M. Copic, and A. Mertelj, Phys. Rev. E **106**, 021001 (2022).

[55] N. Atzin, A. Mozaffari, X. Tang, S. Das, N. L. Abbott, and J. J. de Pablo, Phys. Rev. Lett. **131**, 188101 (2023).

[56] X. Tang, N. Atzin, A. Mozaffari, S. Das, N. L. Abbott, and J. J. de Pablo, ACS Nano **18**, 10768 (2024).